Bulletin of Earthquake Engineering
https://doi.org/10.1007/s10518-024-01955-4

ORIGINAL ARTICLE

# Fragility functions for non-ductile infilled reinforced concrete buildings using next-generation intensity measures based on analytical models and empirical data from past earthquakes

**Al Mouayed Bellah Nafeh**[1] · **Gerard J. O'Reilly**[1]

Received: 12 April 2024 / Accepted: 8 June 2024


**Abstract**
The regional seismic risk assessment of reinforced concrete (RC) building portfolios is a critical issue in earthquake engineering due to their high vulnerability and widespread distribution in seismic prone areas. A pertinent aspect in regional seismic risk applications is the ability to accurately quantify the exceedance of any damage state, generally via fragility functions. To this end, this study derives analytical fragility functions for large-scale seismic risk applications of non-ductile RC buildings with masonry infills characteristic of the Italian peninsula and Southern Europe in general. These were derived using a large database of archetype buildings developed to represent the temporal evolution in construction practice in Italy based on an extensive literature review and interviews with practising engineers and architects. Fragility functions for several infilled RC taxonomy classes were derived for multiple damage states using state-of-the-art analysis on detailed numerical models. Average spectral acceleration was adopted as the intensity measure throughout, since it has been shown to notably reduce dispersion and bias in quantifying the response, and subsequently refine the seismic risk estimates, for these typologies. The fragility functions are compared against empirical data collected following past earthquakes in Italy, namely L'Aquila 2009 and Umbria-Marche 1997. The development of empirical fragility functions was carried out using a novel derivation of average spectral acceleration-based ground-motion fields considering spatial and cross-period correlation models, which is a key component and development in this study. This paper shows how recent advances in analytical fragility function development can be integrated with past empirical observations to give more accurate and representative damage estimates for regional assessment.

**Keywords** Seismic risk · Fragility functions · Analytical models · Empirical data

✉ Gerard J. O'Reilly
gerard.oreilly@iusspavia.it

Al Mouayed Bellah Nafeh
mouayed.nafeh@iusspavia.it

[1] Centre for Training and Research on Reduction of Seismic Risk (ROSE Centre), Scuola Universitaria Superiore IUSS Pavia, Palazzo del Broletto, Piazza della Vittoria 15, 27100 Pavia, Italy

Published online: 21 June 2024

## 1 Introduction

Infilled reinforced concrete (RC) buildings represent a large proportion of the building stock in Italian and Southern Mediterranean seismic-prone regions. Additionally, a significant number of infilled RC buildings were constructed before the introduction of modern seismic guidelines [e.g., NTC (2018) in Italy or Eurocode 8 (Standard 2004)]. For example, buildings constructed in Italy before the 1970s were typically designed to resist gravity loads only with no consideration for ductile detailing or capacity design principles. Gravity load-designed (GLD) buildings were mainly designed utilising the allowable stress method in design. The period between the mid-1970s and 1980s witnessed the implementation of the equivalent lateral force (ELF) method. ELF, as implemented in that period, was a substandard static design (SSD) procedure where lateral forces are calculated as product of a seismic coefficient, defined as around 7–10%, and the weight of structures, as described by Crowley et al. (2021). Additionally, masonry infill panels were typically neglected in the design process and their effects on the structural system's response were generally thought to be a conservative benefit. However, past experimental (Morandi et al. 2018; Kurukulasuriya et al. 2022), analytical (Dolšek and Fajfar 2008; Fardis and Calvi 1994) and field observations (Ioanna et al. 2012; Parisi et al. 2012) have highlighted the detrimental effect of infill panels on the global response and their impact on the vulnerability to ground shaking for infilled RC buildings.

Within the earthquake engineering community, the term seismic risk is a measure of seismic hazard's impact on the built environment. Seismic risk can be quantified in various forms such as expected losses, probability or annual rate of exceeding a given level of consequence. The Pacific Earthquake Engineering Research (PEER) Center's performance-based earthquake engineering methodology (Cornell and Krawinkler 2000; Krawinkler and Miranda 2004) offers a conceptual formulation to incorporate the uncertainties at each stage of analysis via:

$$\lambda(DV > x) = \int_{DM}\int_{EDP}\int_{IM} P(DV > x|DM)f(DM|EDP)f(EDP|IM)|dH(IM)|dEDPdDM \tag{1}$$

where $DV$ is a decision variable, $\lambda(DV > x)$ is the annual rate of $DV$ exceeding a threshold $x$; $DM$ is the vector of damage measures indicating the discrete damage states (DSs) of each component in the building; EDP is the vector of engineering demand parameters, such as storey drift and peak floor acceleration demands in the building; IM is the ground-motion intensity measure level; $dH(IM)$ is the hazard curve derivative, and $f(a|b)$ is a conditional probability distribution function for $a$ given $b$.

This formulation breaks down seismic risk evaluation into separate modules, making it conducive to interdisciplinary investigations. While initially developed to conduct localised seismic risk assessment of individual structures, the framework has progressively found use in risk-based design (e.g., O'Reilly et al. 2022; Fox and O'Reilly 2023; Gentile and Calvi 2023) and regional seismic risk applications (e.g., Heresi and Miranda 2023; Kohrangi et al. 2021; Silva et al. 2015; Padgett et al. 2010; Mangalathu and Jeon 2020; Ruggieri et al. 2022, 2023) to evaluate the seismic hazard effects on spatially distributed structure and infrastructure systems. Risk assessment comprises four key analysis components: (1) exposure modelling characterising physical assets in terms of their structural features, spatial positioning, connections, and occupancy; (2) seismic hazard analysis that estimates earthquake exceedance probability for a given ground shaking intensity; (3) fragility

assessment that evaluates the probability of structural DS being exceeded, considering ground motion intensity and other structure-specific factors; and (4) consequence assessment estimating both direct and indirect seismic losses quantitatively, including economic impacts, casualties, recovery time, etc. Therefore, a key ingredient of regional seismic risk assessment is the adequate characterisation of physical asset vulnerability. This requires quantifying the exceedance probability of any structural demand-based performance level, or limit state, typically quantified with fragility functions (FFs).

The IM represents the interface between the probabilistic seismic hazard analysis (PSHA) and risk analysis. The most commonly used IMs in current practice are the peak ground acceleration (PGA), or the 5%-damped pseudo-acceleration spectral acceleration at a given period, $Sa(T)$. This is generally due to the high availability of ground-motion models (GMMs) for these IMs and their use in seismic design provisions. For example, in Italy, many studies have used these conventional IMs in the past three decades in regional seismic risk applications (Rota et al. 2008, 2011; Gaudio et al. 2017, 2016; Rosti et al. 2021; Borzi et al. 2008; Manfredi et al. 2023). Yet, despite the practicality of conventional IMs, these studies have commonly observed significant uncertainty in the FFs when using these IMs, which is usually indicative of poor IM efficiency. Moreover, additional studies have highlighted notable shortcomings of PGA and $Sa(T)$ for estimating seismic demands in multi-degree-of-freedom systems with non-linear behaviour, leading to large uncertainties and significant bias in the response estimation (O'Reilly 2021; Dávalos and Miranda 2019).

This study develops novel analytical FFs for large-scale (regional) seismic risk applications of non-ductile RC buildings with masonry infills characteristic of the Italian peninsula and Southern Europe in general. Distinct sub-taxonomies were considered based on attributes affecting seismic vulnerability, such as the number of storeys and design code level. FFs for several sub-taxonomy classes were derived for multiple DSs using extensive non-linear time-history analysis on a large database of archetype buildings representative of pre-1970s and 1980s construction practice in Italy. The analytical FFs were then compared against empirical data collected for this structural typology in two past earthquakes in Italy, namely the Umbria-Marche 1997 and L'Aquila 2009 earthquake, to show how recent advances in analytical FF development can be integrated with past empirical observations to give more accurate and representative damage estimates for regional assessment. A summary of the proposed framework adopted in the study herein is presented in Fig. 1.

## 2 Derivation of fragility functions from analytical models

Fragility functions probabilistically quantify the vulnerability of structures to seismic hazards and are often derived from numerical models (Manfredi et al. 2023; Sousa et al. 2021; Giordano et al. 2021; Olteanu et al. 2016; Karim Zadeh et al. 2022), herein referred to as analytical FFs. The key steps to derive analytical FFs are summarised below and described in subsequent sections:

- Step 1: Definition of taxonomies (i.e., building classes) of interest and development of archetype numerical building models
- Step 2: Definition of DSs and EDP-based thresholds for damage assessment
- Step 3: Seismic hazard characterisation, intensity measure selection and ground-motion record selection

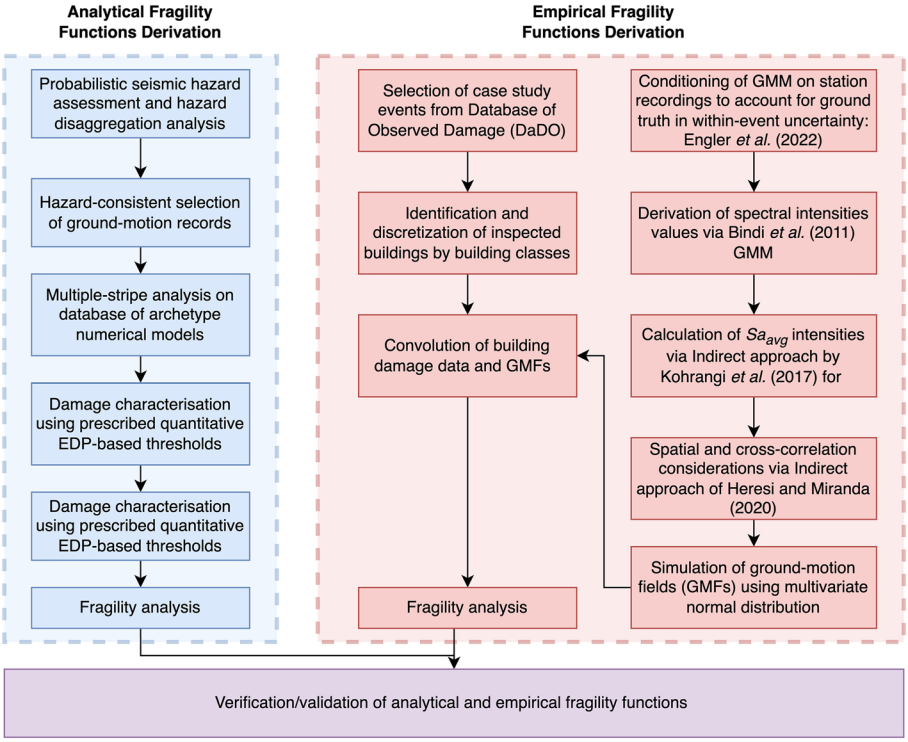


**Fig. 1** Flowchart illustrating the steps required for the derivation of analytical and empirical fragility functions carried out in this study

- Step 4: Response characterisation of the archetype building models via non-linear dynamic analysis
- Step 5: Derivation of analytical FFs using robust statistical methods

## 2.1 Definition of taxonomies and database of archetype building models

A building taxonomy is a key step towards assessing seismic risk and it is generally organised as a series of subsets of classes, referred to herein as sub-taxonomies. For example, infilled RC buildings constructed before the 1970s are a sub-taxonomy of infilled RC buildings. Sub-taxonomies are defined using building attributes relevant to seismic vulnerability, such as load-bearing system, lateral load-resisting system, height or date of construction. Taxonomies should be simple to remain familiar and applicable to other users, but also comprehensive to maintain relevance in how they describe the seismic performance of different construction types.

Based on census data available from the Italian National Institute of Statistics (ISTAT) (Verdi et al. 2011), the sub-taxonomies presented in this study were defined using two prominent attributes: number of storeys (low-rise and mid-rise) and design code level (low-code and moderate-code). The latter also implicitly accounts for the period of construction and ductility levels. The temporal distribution of RC buildings within the Italian building stock based on their distinct attributes is shown in Fig. 2. Similar definitions were also

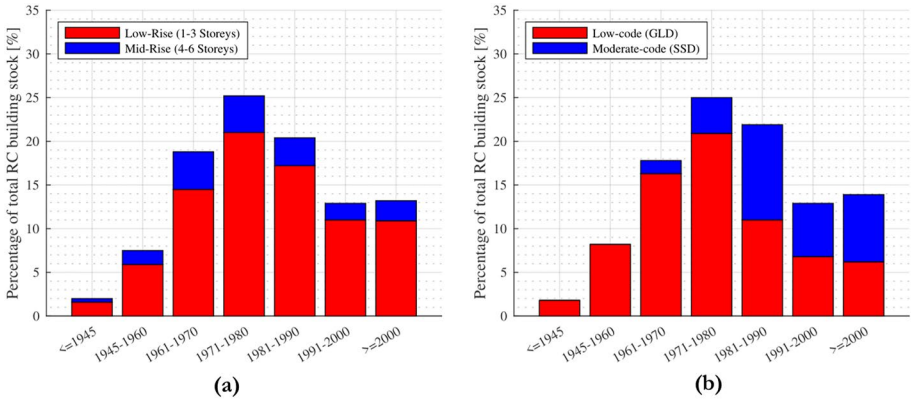


**Fig. 2** Italian RC building stock temporal distribution based on the **a** number of storeys and **b** design code level

adopted within European seismic risk frameworks, such as SERA (2018). Their description is provided in Table 1 and for the sake of brevity, the defined sub-taxonomies will be referred to herein by their codes listed in Table 1.

Assessing the seismic performance of structures generally involves analysing numerical models representative of the structural typology being investigated, generally referred to as archetype building models. Guidelines such as FEMA P695 (2009) recommend that archetype-building models encompass a wide range of design requirements, including the construction period, the corresponding design practices, the gravity and lateral-load bearing structural system, variability in material properties, occupancy type and intended use, building height, elevation and plan configuration, for example. To this end, a database of archetype-building models for infilled RC frames was developed by the authors (Nafeh and O'Reilly 2022) and is available on GitHub (O'Reilly and Nafeh 2021). This database was adopted here and considers two temporal design practices: pre-1970s, where buildings were designed to resist gravity loads only (i.e., low-code or LC in Table 1), and post-1970s, where seismic design was carried out using the ELF method (i.e., moderate-code or MC in Table 1) where a lateral force coefficient of 7–10% was typically considered depending on the seismic zonation. These buildings were mainly designed using the Royal Decree 2229/39 (1939) with complementary references, utilising the allowable stress method in design (Santarella 1957; Pagano 1977). For this application, a seismic coefficient of 7% was considered based on past literature. The design space features were identified using ISTAT housing census data (Verdi et al. 2011) and for complete design information, readers are referred to Nafeh and O'Reilly (2022).

Numerical models of the archetype buildings were developed in OpenSees (McKenna 2011) using the three-dimensional lumped plasticity approach described in O'Reilly and Sullivan (2019). Beams and columns were modelled as elastic elements with cracked section properties and concentrated plastic hinges at the member ends. Empirical calibrations from various sources were employed to determine strength, deformation capacities, and hysteresis parameters for different beam-column types. The flexural response was simulated using rotational springs and a *Pinching4* material model available in OpenSees. Shear strength was integrated by coupling flexural and shear springs at plastic hinges, which allowed premature shear failures to be captured. Staircase elements were included to

**Table 1** Infilled RC building sub-taxonomies adopted in this study

| Building class | Sub-taxonomy code | Description | Number of building models considered |
|---|---|---|---|
| GLD low-rise infilled RC buildings | LC-LR | LC (low-code): refers to structures designed for gravity loads only and allowable stress method with no consideration of ductile detailing | 14 |
| GLD mid-rise infilled RC buildings | LC-MR | MR (mid-rise): refers to structures with 4–6 storeys above ground | 21 |
| SSD low-rise infilled RC buildings | MC-LR | LR (low-rise): refers to structures with 1–3 storeys above ground | 14 |
| SSD mid-rise infilled RC buildings | MC-MR | MC (moderate-code): refers to structures designed according to the ELF method with a seismic coefficient of 7%, the allowable stress method and no consideration of ductile detailing | 21 |

consider added stiffness and torsional behaviour in the global dynamic response. For beam-column joints, empirical relationships from Risi and Verderame (2017) and Risi et al. (2017) and O'Reilly and Sullivan (O'Reilly and Sullivan 2019) were applied to exterior and interior joints in non-ductile structures. Infill panels were modelled using the equivalent strut approach (Crisafulli and Carr 2007), offering single and double strut options to account for shear caused by the frame-panel interaction. Infill strength variations followed the categorisation in Hak et al. (2012). An example of one of the building models is illustrated in Fig. 3 and further details on the numerical modelling can be found in Nafeh and O'Reilly (2022).

## 2.2 Damage state definition

Damage states are widely used in seismic risk applications to relate observed structural damage to consequences like building functionality, economic losses and possible casualties. FFs express the exceedance probability of a certain DS as a function of seismic shaking intensity. Therefore, the derivation of FFs requires the ability to accurately quantify the exceedance of any structural demand-based DS. In practical applications, DSs are typically referred to as limit states and are triggered by several potential factors, both on a local and global level. This can be either global displacement-based, local deformation-based or local strength-based criteria. For example, the Italian national code (NTC2018 2018) identifies four limit states based on the lateral capacity of the main structural system. Their quantitative descriptions for RC frames structures with infills are given in the NTC2018 commentary (MINISTERO DELLE INFRASTRUTTURE E DEI TRASPORTI. CIRCOLARE 2019) and are briefly summarised below:

- Stato Limite di Operatività 'Operational' (SLO): Structural and non-structural elements maintain functionality without suffering damage and significant interruption. Moderate damage to infill panels is foreseen at low levels of drift. The SLO limit state corresponds to the exceedance of a global storey drift, $\theta_{max}$, of 0.33%;
- Stato Limite di Danno 'Damage Control' (SLD): Structural and non-structural elements suffer moderate damage. The structure remains under immediate occupancy

without jeopardising human life. The overall capacity and stiffness of the structure are not compromised. The SLD limit state corresponds to the first exceedance of the yield chord rotation, $\theta_y$, in either beam or column elements or the exceedance of a global storey drift, $\theta_{max}$, of 0.50%;

- Stato Limite di salvaguardia della Vita 'Life Safety' (SLV): The structure sustains heavy damage to its structural elements, resulting in a significant loss of lateral stiffness. The structure retains its gravity load-carrying capacity with a margin of safety against collapse. Failure of non-structural elements is a direct consequence of attaining SLV. The SLV limit state corresponds to the exceedance of 75% of the ultimate chord rotation, $\theta_{ult}$, or the yield shear capacity, $V_y$, in any beam or column element in the building, or the yield capacity of any beam-column joint;
- Stato Limite di prevenzione del Collasso 'Collapse Prevention' (SLC): Structural and non-structural elements suffer heavy damage. The structure maintains gravity-load carrying capacity with a slender margin of safety against collapse due to the full exploitation of the strength and deformation capacity. The SLC limit state is attained when a residual capacity of 80% of the maximum base shear is achieved, or the ultimate chord rotation is exceeded in any component (i.e., beam, column and joint).

Since the typology under consideration in this work is non-ductile infilled RC frames, these DSs are also impacted by the premature failure of the infill panels and the degradation in strength due to the in-plane–out-of-plane (IP–OOP) interaction (Milanesi et al. 2021; Morandi et al. 2022). However, this study focuses solely on the in-plane failure of the masonry panels and the effects of the in-plane out-of-plane interaction (Kurukulasuriya et al. 2022; Morandi et al. 2022) were not considered due to current numerical modelling limitations. However, experimental tests, both in-plane and out-of-plane, carried out by Kurukalasuriya et al. (2023) demonstrated that for infilled RC frame buildings, the initial DSs (i.e., SLO and SLD) are governed by the in-plane drifts sustained by the infill panels. These correspond to storey drift values of 0.16% and 0.29% for the SLO and SLD limit states, respectively. To account for this, a hybrid definition of DS thresholds was adopted in this study, where the findings of Kurukalasuriya et al. (2023) were adopted for the SLO and SLD limit states, and NTC18-based guidelines were adopted for the definition of the SLV and SLC criteria, where the structural capacity of the frame members would be expected to play a key role. An additional collapse limit state was considered, where complete collapse

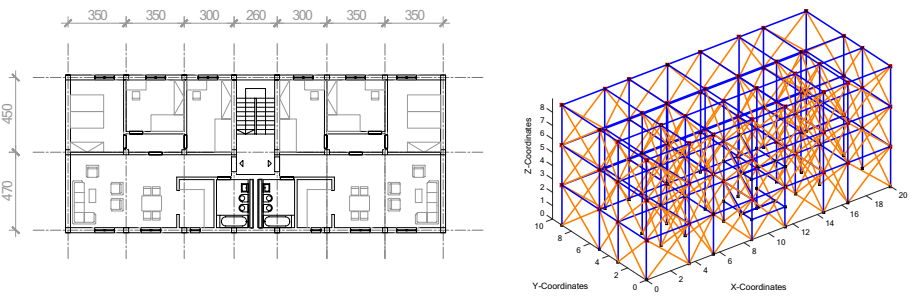


(a) (b)

**Fig. 3** **a** Plan layout, where dimensions are in cm, and **b** OpenSees numerical model of an archetype building, where dimensions are in m

of the structure is expected. This is taken to be when 5% storey drift is exceeded in non-linear dynamic analyses, as discussed by O'Reilly et al. (2018). Table 2 summarises the quantitative DS definitions adopted herein, where those from the NTC2018 building code commentary are also reported for reference. These definitions will be key when comparing them to more qualitative definitions of damage utilised in empirical data collection, which is discussed in Sect. 3.

### 2.3 Seismic hazard characterisation and intensity measure selection

Deriving robust FFs entails selecting a suitable IM to characterise the relationship between damage and shaking intensity accurately. Several recent studies have proposed alternative IMs with higher efficiency, sufficiency, and predictability than PGA or $Sa(T_1)$ (Dávalos and Miranda 2019; Marafi et al. 2016; Biasio et al. 2014; Eads et al. 2015). Compared to more traditional IMs, the average spectral acceleration, or $Sa_{avg}$, (Vamvatsikos and Cornell 2005; Eads et al. 2015) is appealing given its demonstrated efficiency and sufficiency properties (O'Reilly 2021; Nafeh and O'Reilly 2022; Heresi and Miranda 2021), which in return made it favourable in several studies (O'Reilly 2021; Nafeh and O'Reilly 2022, 2023; Kohrangi et al. 2017; Qian and Dong 2020). It is defined as:

$$Sa_{avg}(T^*) = \left( \prod_{i=1}^{N} Sa(c_i T^*) \right)^{1/N} \tag{2}$$

where $c_i$ represents $N = 10$ number coefficients in the range of 0.2–3.0 and $T^*$ is the conditioning period. In addition to $Sa_{avg}(T^*)$ delivering high efficiency and sufficiency, the range of periods considered in its definition represents an important advantage for regional seismic risk assessment because each asset's vibration period within a building stock is usually an unknown quantity. More importantly, from the computational and practical point of view, it allows the use of the same IM over the whole region of interest instead of using different IMs for different structures (Heresi and Miranda 2021).

Seismic hazard analysis involves characterising earthquake rupture sources at a specific site of interest and identifying the relationship between these rupture characteristics and the intensity of ground shaking via an IM. OpenQuake (Pagani et al. 2014) can be used to conduct PSHA, where the annual probability of exceeding an IM level at a given site location is obtained. In this study, the archetype buildings were assumed to be located in the city of L'Aquila, Italy, and the most recent European seismic hazard model (ESHM20) (Danciu et al. 2020) was used with the site characteristics presented by Mori et al. (2020)

**Table 2** Damage state criteria according to the current NTC2018 local and global strength and deformation criteria and those adopted in this study

| Damage state | NTC 2018 criteria | Adopted thresholds |
|---|---|---|
| SLO | $\theta_{max} = 0.33\%$ | $\theta_{max} = 0.16\%$ |
| SLD | min $\{\theta_{y,beam}; \theta_{y,column}\}$ | $\theta_{max} = 0.29\%$ |
| SLV | min $\{0.75\theta_{ult,beam}; 0.75\theta_{ult,column}; V_{y,beam}; V_{y,column}, M_{y,\,joint}\}$; | min $\{0.75\,\Delta_{roof,SLC}; 0.75\,\theta_{ult,beam}; 0.75\theta_{ult,column};\}$ |
| SLC | min $\{0.80\,V_{\max}; \gamma_{ult,joint}; \theta_{ult,beam}; \theta_{ult,column}\}$ | min $\{0.80\,V_{\max}; \theta_{ult,beam}; \theta_{ult,column}\}$ |
| Collapse | – | $\theta_{max} = 5.0\%$ |

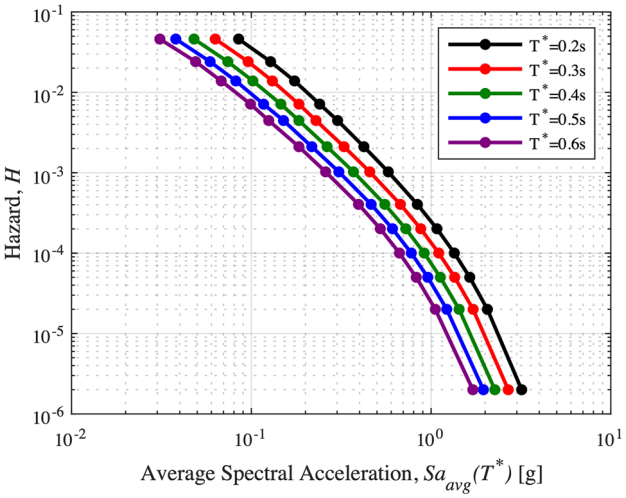


**Fig. 4** Seismic hazard curves based on average spectral acceleration, $Sa_{avg}(T^*)$, for L'Aquila, Italy

to estimate the seismic hazard curves for different definitions of $Sa_{avg}(T^*)$, which are illustrated in Fig. 4.

### 2.4 Non-linear dynamic analyses

Multiple-stripe analyses (MSA) (Jalayer and Cornell 2009) were carried out to individually characterise the non-linear dynamic response of the archetype buildings at discrete intensity levels. MSA is a standard dynamic analysis procedure that uses the conditional spectrum (Baker 2011) to select suitable ground-motion records consistent with the site hazard at each intensity level. This is due to the change in causative rupture parameters of the ground motion records with increasing intensity levels (Bradley 2010; Lin et al. 2013). To this end, hazard disaggregation analysis was carried out to identify the most representative rupture scenarios for a given IM and return period. A suite of 25 records per intensity was selected considering five conditioning periods, $T^*$, for $Sa_{avg}(T^*)$ which were in the range of the geometric mean of the first-mode periods of vibration (i.e., $T^* = \sqrt{T_{1,x}T_{1,y}}$) for the two to six storey buildings, giving the hazard curves for $T^* = 0.2$–$0.6$ s shown in Fig. 4. Nine intensity levels corresponding to return periods of 22 to 4975 years were analysed to characterise structural response from initial damage of the masonry infill panels up to global structural collapse. The minimum and maximum scaling factor thresholds for record selection were limited to 1.0 and 2.0, respectively. An excerpt of the MSA results is presented in Fig. 5, where the structural response was characterised in terms of the maximum peak storey drift, $\text{EDP} = \theta_{\max}$, with increasing levels of $\text{IM} = Sa_{avg}(T^*)$.

A drawback of MSA for this application is that each archetype building model was evaluated using a slightly different definition of $Sa_{avg}(T^*)$. For example, the MSA results for buildings ranging from 2 to 3 storeys with fundamental periods of 0.2–0.3 s cannot be collectively considered when assuming one sub-taxonomy. To characterise the overall seismic performance of an entire sub-taxonomy, it is necessary to assess

buildings using the same IM. Therefore, it is necessary to group buildings pertaining to a defined sub-taxonomy using a common IM. $Sa_{avg}(T^*)$ was again chosen as the IM and the conditioning period of taxonomy, $T^*_{tax}$ was defined as the geometric mean of the periods within the sub-taxonomy. For example, the LC-LR sub-taxonomy consists of two- and three-storey buildings with $T^*$ of 0.2 and 0.3 s, respectively. Therefore, the equivalent conditioning period of the LC-LR sub-taxonomy would be equal to $T^*_{tax} = \sqrt{0.2 * 0.3} \approx 0.25s$. The taxonomy-based conditioning period values are reported in Table 3.

As a result of the building grouping, results of MSA carried out on individual buildings would change given the shift in IM definition from $Sa_{avg}(T^*)$ to $Sa_{avg}(T^*_{tax})$ and therefore new spectral intensities must be determined. To do so, the spectral intensities associated with $Sa_{avg}(T^*_{tax})$ were computed from the spectra of each ground-motion record used in the structure-specific MSA. While new spectral intensities are calculated, no changes to the EDP value are needed. As such, the striped results of MSA highlighted in Fig. 5a would transform into a "banded cloud" of results similar to results achieved following a cloud analysis as shown in Fig. 5b. The results are still largely hazard-consistent since although the results are now being reconditioned on $Sa_{avg}(T^*_{tax})$, from the individually-selected ground motions in terms of $Sa_{avg}(T^*)$, the hazard-consistency across all periods close to $T^*$ ensures this is not overly problematic. Alternatively, to avoid this re-conditioning of MSA results, a more direct approach could have been to directly select ground motion records for MSA in terms of $Sa_{avg}(T^*_{tax})$. Therefore, cloud analysis was used, as illustrated in Fig. 5b. Furthermore, Fig. 5b demonstrates two regression lines, depicted with black and blue solid lines, representing traditional cloud analysis and modified cloud analysis, respectively. In Fig. 5b, green scatter indicates non-collapse cases ($\theta_{max} < 5.0\%$) while red scatter represents collapse cases ($\theta_{max} \geq 5.0\%$). Both approaches aim to evaluate the probabilistic seismic demand on structures, but they differ in handling the relationship between ground motion intensity and structural response. Traditional cloud analysis (Jalayer et al. 2017) uses a simpler, typically linear approach and censors collapse cases. In contrast, modified cloud analysis explicitly includes collapse cases, modeling the probability of collapse using logistic regression and updating the non-collapse regression to account for this probability.

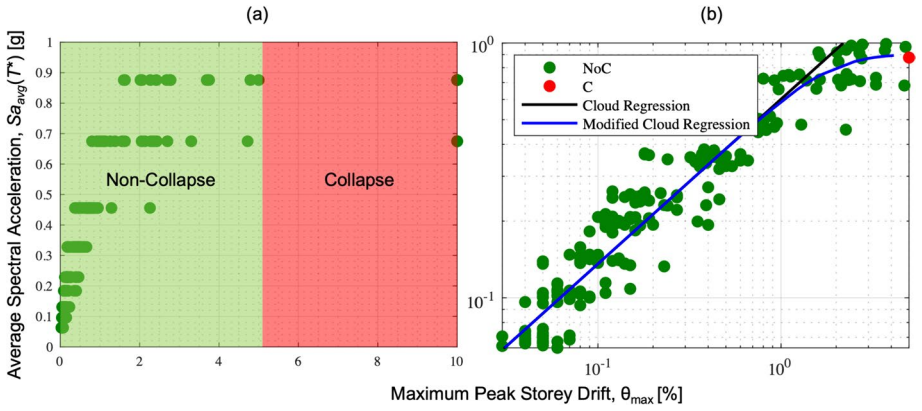


**Fig. 5** **a** Multiple-stripe analysis and **b** cloud analysis results for a LC-LR building from the archetype database of infilled RC buildings. Non-collapse and collapse cases are indicated in green and red, respectively

### 2.5 Analytical fragility functions

A lognormal distribution is typically used to characterise FFs used in seismic vulnerability analysis. Lognormality is a common assumption that has been shown to provide adequate results in various studies (Porter et al. 2007; Eads et al. 2013; Bradley and Dhakal 2008). As such, FFs are described by a median seismic intensity, $\eta$, and an associated dispersion, $\beta$. In this context, the former is defined as the seismic intensity required to observe 50% exceedances of any given EDP-based threshold, whereas the latter accounts for sources of uncertainty, namely epistemic and aleatory. Following the identification of both components, the FFs are defined as per Eq. 3:

$$P\left[x \geq DS_i | IM = im\right] = \Phi\left(\frac{\ln\left(im/\eta_i\right)}{\beta_i}\right) \tag{3}$$

where $P\left[x \geq DS_i | IM = im\right]$ is the probability that a ground motion intensity with IM = $im$ will cause the structure to exceed a particular damage state $i$ ($DS_i$); $\Phi()$ is the standard normal cumulative distribution function; $\eta_i$ and $\beta_i$ are the median and the associated standard deviation of the FF at $DS_i$, respectively.

#### 2.5.1 Building-specific fragility functions

Following the dynamic analysis on individual archetype numerical models, the median seismic intensity required to observe 50% exceedances of any given EDP-based threshold or $\eta_{IM|EDP}$, a linear regression in log-space can be carried out (Jalayer et al. 2015) as illustrated in Fig. 5b for a single case and whose functional form is reported in Eq. 4:

$$\ln\eta_{IM|EDP} = \ln a + b\ln EDP \tag{4}$$

where for a known EDP-based definition of the $DS_i$, the median value for a building $j$ can be determined as $\eta_{IM|EDP,j,DS_i}$. In cloud analysis, the uncertainty in the quantified IM given EDP, also termed record-to-record variability, $\beta_{RTR}$, is a single constant value across the range of structural response for a given building $j$ and corresponds to the standard deviation associated with the regression carried out to characterise the IM-EDP relationship in log-space, or $\sigma_{\ln IM|EDP,j}$, and is computed as:

$$\beta_{RTR,j} = \sigma_{\ln IM|EDP,j} = \sqrt{\frac{\sum_{g=1}^{N_{gms}}\left(\ln im_g - \ln\eta_{IM|EDP,j}\right)^2}{n-2}} \tag{5}$$

where $\eta_{IM|EDP,j}$ is the median IM value associated with the fitted linear regression model (blue line in Fig. 5b); $im_g$ are the IM values associated with the scatter or cloud of points (individual green scatter points in Fig. 5b) for each ground motion $g$. Herein, $im_g$ corresponds to the $Sa_{avg}(T^*)$ value of ground motion $g$; and $N_{gms}$ is the number of ground motion records.

The result of this is that the FFs for each building $j$ and each DS $i$ are characterised by a median, whose value is computed directly from the fitted linear regression in Eq. 4 depending on the damages state's EDP value, and a constant value of dispersion for all damages states, as per Eq. 5.

**Table 3** Definition of periods used to describe $Sa_{avg}(T^*_{\text{tax}})$ for each sub-taxonomy

| Sub-taxonomy code | Individual buildings<br>Conditioning period, $T^*$ | Grouped buildings<br>Conditioning period, $T^*_{tax}$ |
|---|---|---|
| LC-LR | 0.2 s and 0.3 s for two- and three-storey buildings, respectively | $\sqrt{0.2 * 0.3} \approx 0.25s$ |
| LC-MR | 0.4 s, 0.5 s and 0.6 s for four-, five- and six-storey buildings, respectively | $\sqrt[3]{0.4 * 0.5 * 0.6} \approx 0.50s$ |
| MC-LR | 0.2 s and 0.3 s for two- and three-storey buildings, respectively | $\sqrt{0.2 * 0.3} \approx 0.25s$ |
| MC-MR | 0.4 s, 0.5 s and 0.6 s for four-, five- and six-storey buildings, respectively | $\sqrt[3]{0.4 * 0.5 * 0.6} \approx 0.50s$ |

### 2.5.2 Taxonomy-based fragility functions

Moving from building-specific FFs to taxonomy-based FFs requires consideration of the individual building-specific lognormal distribution parameters to assess the resulting taxonomy-based parameters. This transition was previously carried out by Abarca et al. (2022) and Ruggieri et al. (2021) among others, using the law of total variance.

First, the taxonomy-based median seismic intensities associated with the exceedance of a DS threshold or $\widetilde{\eta}_{IM|EDP,DS_i}$ are evaluated. Simply put, this value corresponds to the mean of the individual median seismic intensities associated with the exceedance of different DS thresholds for each building (Eq. 4) computed as:

$$\widetilde{\eta}_{IM|EDP,DS_i} = \frac{1}{N}\sum_{j}^{N_{bdgs}} \eta_{IM|EDP,j,DS_i} \tag{6}$$

Moreover, the seismic performance assessment of any given structural typology requires due consideration of both aleatory and epistemic sources of uncertainty. The former is generally associated with the randomness in ground motion records, whereas the latter typically relates to uncertainties in the numerical modelling. In this study, the overall dispersion associated with the mean lognormal FFs of each taxonomy and each DS *i*,

$\widetilde{\beta}_{total|DS_i}$ was derived as per the law of total variance by considering the intra-building, $\widetilde{\beta}_{intra}$, that is a constant value for all DSs given the homoscedasticity assumption adopted in Eq. 5, and the inter-building, $\widetilde{\beta}_{inter|DS_i}$, dispersions of the median values presented in Eqs. 7 and 8, respectively. These are described via:

$$\widetilde{\beta}_{intra} = \sqrt{\frac{1}{N_{bdgs}}\sum_{j=1}^{N_{bdgs}} \beta^2_{RTR,j}} \tag{7}$$

$$\widetilde{\beta}_{inter|DS_i} = \sqrt{\frac{1}{N_{bdgs}}\sum_{j=1}^{N_{bdgs}} \left(\ln\eta_{IM|EDP,j,DS_i} - \ln\widetilde{\eta}_{IM|EDP,DS_i}\right)^2} \tag{8}$$

where $\ln\eta_{IM|EDP,j,DS_i}$ is the seismic intensity required to exceed a certain DS threshold *i* for an individual building *j*, $\ln\widetilde{\eta}_{IM|EDP,DS_i}$ is the mean seismic intensity for a group of buildings

of similar characteristics computed via Eq. 6, and $N_{bdgs}$ is the total number of buildings per taxonomy and $DS_i$ denotes the damage state of interest.

In addition to the noted sources of uncertainties, the uncertainty associated with the modelling parameters for existing RC building numerical modelling or $\beta_{MDL}$ should also be accounted for in the overall dispersion (Eq. 9). Various studies investigated the modelling uncertainty. For example, Mucedero et al. (2022) have investigated the effects of masonry infill variability and RC shear failure on the overall epistemic uncertainty where $Sa_{avg}$ was considered as the IM, although relatively high values of dispersion were reported. Furthermore, O'Reilly and Sullivan (2018) examined several buildings for existing RC frames with masonry infills designed before the introduction of seismic design provisions in Italy. O'Reilly and Sullivan (2018) suggest values between 0.19 and 0.34 depending on the infill typology (i.e., weak or strong infills) and the number of storeys, which is more in line with other studies and recommendations (FEMA 2012). Subsequently, a value of $\beta_{MDL}$=0.34 was utilised for the two- to six-storey infilled RC frame structures. The total dispersion is then computed as:

$$\widetilde{\beta}_{total|DS_i} = \sqrt{\widetilde{\beta}^2_{intra} + \widetilde{\beta}^2_{inter|DS_i} + \beta^2_{MDL}} \tag{9}$$

where Appendix provides further information on the assumptions and limitations of this combination. Basically, Eq. 9 holds so long as the modelling uncertainty is assumed to not impact the median values and it is a constant value across all buildings for a given damage state. The taxonomy-based FFs can then be defined via the median value $\widetilde{\eta}_{IM|EDP,DS_i}$ (from Eq. 6) and the total dispersion $\widetilde{\beta}_{total|DS_i}$ (from Eq. 9).

$$P\left[x \geq DS_i | IM = im\right] = \Phi\left(\frac{\ln\left(im/\widetilde{\eta}_{IM|EDP,DS_i}\right)}{\widetilde{\beta}_{total|DS_i}}\right) \tag{10}$$

### 2.5.3 Proposed analytical fragility functions

To demonstrate the evaluation of the analytical FFs described in the previous subsection, an example calculation is reported in Table 4 where the equations previously presented were applied to estimate of the taxonomy-based median DS seismic intensities evaluated using building-specific analysis results and the total uncertainty associated with a taxonomy for a given damage state *i*. The example provided in Table 4 corresponds to the collapse DS for the low-code low-rise infilled RC building class (i.e., the black line in Fig. 6a).

The entire set of analytical FFs was then plotted for all the considered taxonomies and DSs and presented in Fig. 6, where the ground motion intensities are expressed as a function of $Sa_{avg}$ conditioned on the anchoring period of each taxonomy presented in this study (Table 1). The solid lines represent the combined FFs, whereas the lighter lines represent the individual buildings, where it can be seen how the equations previously presented combine these individual FFs together. The complete set of median intensities and associated dispersions will be presented later in Table 8.

## 3 Derivation of fragility functions from empirical post-earthquake data

Validating analytical FFs with past earthquake events is a crucial step in regional seismic risk analysis. The validation process aims to assess the robustness of the derived analytical FFs in casting future damage estimations. To do so, empirical FFs obtained from observed damage after the occurrence of a significant earthquake event are invaluable since empirical FFs are directly correlated with the actual seismic behaviour of buildings, hence representing a sort of benchmark value. To develop empirical FFs, two key components must be characterised at the location of each building: the mapping of the ground shaking intensity measure values, commonly known as ground-motion fields (GMFs), and the building damage due to this shaking event. A methodology to characterise these fundamental components is discussed in Sects. 3.1 and 3.2, respectively, and methods to incorporate the two elements for the derivation of empirical FFs are outlined in Sect. 3.3. In this study, two seismic sequences (i.e., mainshock plus all recorded aftershocks) in Italy were considered for the validation case study, namely the Umbria-Marche 1997 and L'Aquila 2009 events. These events are well-characterised in terms of scenario characteristics (Table 5), availability of observed damage data and relevance to the taxonomies studied in the previous section. The collection of these registered signals was carried out from the Italian Accelerometric Archive (ITACA, http://itaca.mi.ingv.it) (Pacor et al. 2011a) where recordings belonging to a total of 64 and 118 stations for Umbria-Marche and L'Aquila, respectively, were considered and reported in Table 5 with the designated event ID as documented in the ITACA database.

### 3.1 Ground motion field characterisation

In order to link the observed damage in buildings following an actual earthquake with a seismic intensity, GMFs are required. This is due to the limited amount of actual instrumented recordings in the region, which only provide a partial view of the shaking intensities. Given that it is highly unlikely that each building where damage is observed be equipped with an accelerometer to measure the actual shaking intensity, some inference is needed, which is where GMFs are utilised. These are typically developed following an earthquake event using ground-motion models (MMs) that can predict ground motion intensities where actual recordings are not available. They give a complete estimate of the relative spatial distribution of shaking, generally referred to as ShakeMaps. The methodology for producing GMFs is fully detailed in Worden et al. (2020) and they have a broad range of applications. GMFs are made available online through some institutional facilities such as the Italian National Institute of Geophysics and Volcanology (INGV, http://shakemap.rm.ingv.it/shake4/index.html) or the US Geological Survey (USGS, https://earthquake.usgs.gov/data/shakemap/).

However, one of the major limitations of the GMFs produced and distributed by institutes such as INGV or USGS is their availability for only some IM types, particularly peak ground acceleration, peak ground displacements and the spectral accelerations at 0.3, 1.0 and 3.0 s (i.e., for the periods outlined in the Uniform Building Code). These IM definitions render them a limitation to remedy in this study since $Sa_{avg}$ is utilised, which comprises as the geometric combination of multiple spectral accelerations at distinct periods of vibration and not just a single one. For example, the use of the available spectral intensities at only 0.3, 1.0 and 3.0 s will yield very rough estimates for the calculation of GMFs

**Table 4** Example calculation of the FF parameters the LC-LR sub-taxonomy for the collapse DS

| Building $j$ | $\eta_{IM\|EDP,j,DS_i}$ (Eq. 4) | $\beta_{RTR,j}$ (Eq. 5) | $\widetilde{\eta}_{IM\|EDP,DS_i}$ (Eq. 6) | $\widetilde{\beta}_{intra}$ (Eq. 7) | $\widetilde{\beta}_{inter\|DS_i}$ (Eq. 8) | $\widetilde{\beta}_{total\|DS_i}$ (Eq. 9) |
|---|---|---|---|---|---|---|
| 1 | 1.27 | 0.37 | 1.0078 | 0.31 | 0.19 | 0.50 |
| 2 | 0.79 | 0.38 | | | | |
| 3 | 1.07 | 0.27 | | | | |
| 4 | 0.74 | 0.33 | | | | |
| 5 | 1.16 | 0.34 | | | | |
| 6 | 0.84 | 0.32 | | | | |
| 7 | 1.21 | 0.25 | | | | |
| 8 | 0.85 | 0.27 | | | | |
| 9 | 1.22 | 0.29 | | | | |
| 10 | 0.90 | 0.27 | | | | |
| 11 | 1.19 | 0.37 | | | | |
| 12 | 0.85 | 0.32 | | | | |
| 13 | 1.22 | 0.32 | | | | |
| 14 | 0.80 | 0.28 | | | | |

associated with $Sa_{avg}$. For example, Rosti et al. (2023) have opted to evaluate $Sa_{avg}$ GMFs using physics-based simulations based on the available spectral intensities (i.e., $Sa$(0.3 s), $Sa$(1.0 s) and $Sa$(3.0 s)) using a weight-based method which was dependent on the width of the associated period interval. While the method proposed in Rosti et al. (2023) presented a simplified approach for the calculation of $Sa_{avg}$ GMFs, it does not possess sufficient accuracy and can only be considered a proxy value for $Sa_{avg}$. Therefore, a more refined distribution of spectral intensities is required to accurately characterise GMFs in terms of $Sa_{avg}$. To this end, a procedure to derive $Sa_{avg}$-based GMFs is outlined in the subsequent sections by extending the methods currently utilised.

### 3.1.1 Definition of intensity measure multivariate distribution

To simulate the intensities at each site $j$ for a given rupture event $i$, the distribution of $\ln\boldsymbol{IM}$ is assumed to be described as:

$$\ln\boldsymbol{IM} \sim \mathcal{N}(\boldsymbol{M}, \boldsymbol{\Sigma}) \tag{11}$$

where $\sim \mathcal{N}()$ denotes that $\ln\boldsymbol{IM}$ is multivariate normal distribution, parameterised by the mean vector $\boldsymbol{M}$ and covariance matrix $\boldsymbol{\Sigma}$ defined for $n$ sites as follows:

$$\boldsymbol{M} = \begin{bmatrix} \ln\mu_{IM}\left(rup_i, site_1\right) \\ \ln\mu_{IM}\left(rup_i, site_j\right) \\ \cdots \\ \ln\mu_{IM}(rup_i, site_n) \end{bmatrix} \tag{12}$$

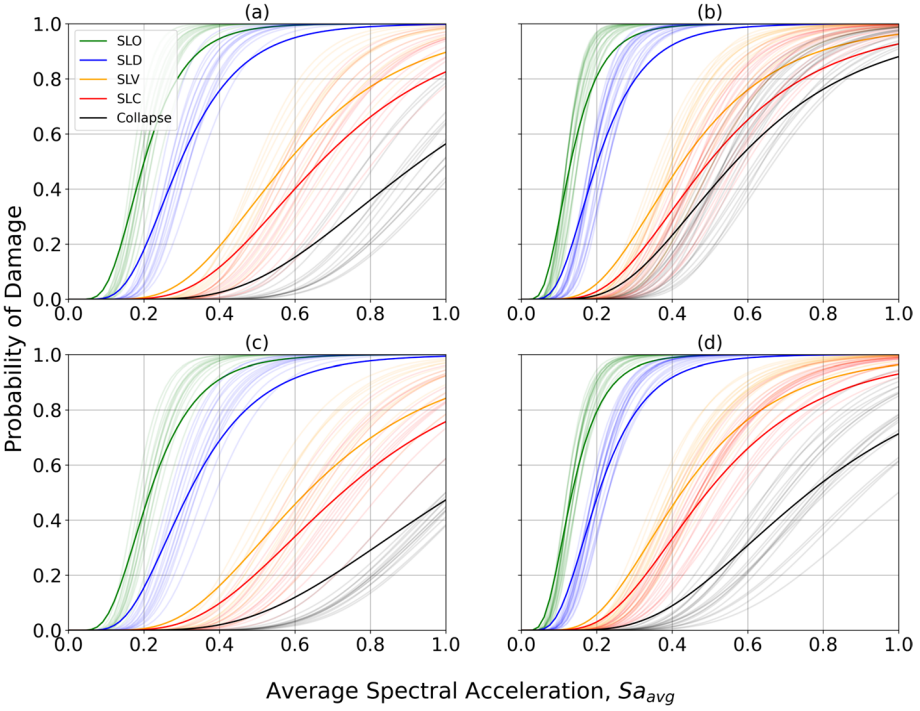


**Fig. 6** Analytical infilled RC FFs for the sub-taxonomies identified in this study expressed in terms of the average spectral acceleration conditioned on the anchoring period of each sub-taxonomy; LC-LR (**a**), LC-MR (**b**); MC-LR (**c**); MC-MR (**d**)

$$\boldsymbol{\Sigma} = \sigma_{inter}^2 1 + \sigma_{intra}^2 \boldsymbol{R} \tag{13}$$

where $\boldsymbol{M}$ is a vector of mean shaking intensity predictions, or $\ln\mu_{IM}\left(rup_i, site_j\right)$, for rupture scenario $i$ at site $j$; $\sigma_{intra}$ and $\sigma_{inter}$ represent the intra- and inter-variability terms, respectively; 1 is a matrix of ones; $\boldsymbol{R}$ is the matrix of within-event correlation coefficients, with diagonal terms equal to unity and off-diagonals equal to the spatial correlation between sites $j$ and $k$, denoted $\rho_{j,k}$, which is assumed to be independent of the rupture characteristics.

The mean ground shaking for rupture $i$ at a given location $j$, $\ln\mu_{IM}\left(rup_i, site_j\right)$, is estimated using a suitably identified GMM for that IM. For this regional application, the GMM proposed by Bindi et al. (2011) was used since it is the one utilised by the INGV for the production of GMFs in Italy. It evaluates the 5%-damped spectral acceleration at a given period, $Sa(T)$ based on the specific rupture characteristics such as magnitude, source-to-site distance, local soil conditions and fault mechanism for the events listed in Table 5. The GMM characterises the inter- and intra-event variabilities (i.e., $\sigma_{inter}$ and $\sigma_{intra}$) along with the total variability, $\sigma_{total}$, which are tabulated in Bindi et al. (2011) as a function of the spectral period.

Following the estimation of the mean shaking terms for different sites, their spatial correlation is an issue that needs to be addressed, as its impacts have been noted to be significant on spatially distributed assets (Wesson 2001; Adachi and Ellingwood 2009; Shiraki et al. 2007; Sokolov and Wenzel 2011; Miano et al. 2016; Lee and Kiremidjian 2007).

**Table 5** List of earthquake events and rupture parameters for the L'Aquila 2009 and Umbria-Marche 1997 sequences

| ITACA event ID | Date and time | Epicentre coordinates | | Magnitude, Mw | Faulting mechanism | Depth [km] | Strike | Dip | Rake |
|---|---|---|---|---|---|---|---|---|---|
| | | Latitude | Longitude | | | | | | |
| *Umbria-Marche 1997* | | | | | | | | | |
| IT-1997-0004 | 26/09/1997 00:33:11 | 43.022500 | 12.891700 | 5.7 | Normal | 5.1 | 152.0 | 46.0 | − 90.0 |
| IT-1997-0006 | 26/09/1997 09:40:24 | 43.081100 | 12.826700 | 6.0 | | 6.8 | 152.0 | 38.0 | − 85.0 |
| IT-1997-0137 | 14/10/1997 15:23:09 | 42.919000 | 12.926000 | 5.6 | | 5.6 | 135.0 | 45.0 | − 90.0 |
| *L'Aquila 2009* | | | | | | | | | |
| IT-2009-0009 | 06/04/2009 01:32:40 | 42.314000 | 13.419300 | 6.1 | Normal | 8.2 | 140.0 | 50.0 | − 90.0 |
| IT-2009-0102 | 07/04/2009 17:47:37 | 42.303000 | 13.486000 | 5.5 | | 17.1 | 346.0 | 63.0 | − 61.0 |

Spatial correlation considers spatial dependence in the joint probability distribution function of an intensity measure given a rupture scenario. A model which does not account for spatial correlation implies that larger-than-median motions would occur at individual locations independently, and lower than average motions may be predicted at an adjacent site, which makes little physical sense. Several phenomena associated with earthquake rupture and wave propagation can produce spatial correlation in the intra-event residuals. To address this issue, the last two decades witnessed a surge in research addressing spatial correlation (Goda and Atkinson 2009; Wang and Takada 2005; Markhvida et al. 2018; Heresi and Miranda 2019; Jayaram and Baker 2009; Esposito and Iervolino 2012; Pavel and Vacareanu 2017) and corresponding to various intensity measures such as PGA, peak ground velocity and, most notably, $Sa(T)$.

Since $Sa_{\text{avg}}$ is used as the IM in this study, a spatial correlation model for this IM is needed, which has to date not been directly quantified. However, taking advantage of the mathematical definition of the IM with respect to $Sa(T)$, the mathematical formulation proposed by Heresi and Miranda (2021) was adopted to compute the $\boldsymbol{R}$ terms as a function of the spatial correlations of $Sa(T)$ at different period, given as:

$$\boldsymbol{R}(j,k) = \rho_{lnSa_{avg,j}lnSa_{avg,k}} = \frac{\frac{1}{100}\sum_{l=1}^{10}\sum_{m=1}^{10}\rho_{lnSa_{l,j},lnSa_{m,k}}.\sigma_{lnSa_{l,j}}.\sigma_{lnSa_{m,k}}}{\sigma_{lnSa_{avg,j}}.\sigma_{lnSa_{avg,k}}} \tag{14}$$

where $\rho_{lnSa_{l,j},lnSa_{m,k}}$ is the cross-correlation between $lnSa_{l,j} = lnSa_j(c_l.T)$ and $lnSa_{m,k} = lnSa_k(c_m.T)$; $\sigma_{lnSa_{l,j}}$ and $\sigma_{lnSa_{m,k}}$ are the standard deviations of $lnSa_{l,j}$ and $lnSa_{m,k}$ obtained from the GMM utilised; $\sigma_{lnSa_{avg,j}}$ and $\sigma_{lnSa_{avg,k}}$ are the standard deviations of $lnSa_{avg,j}$ and $lnSa_{avg,k}$, where the subscript pairs $j$-$k$ and $l$-$m$ denote the sites and the periods, respectively, where the rupture parameters $i$ are assumed to be independent. This essentially represents an indirect means to compute the spatial correlation of $Sa_{\text{avg}}$ at two different sites using the available the spatial correlations of $Sa(T)$ at different periods utilised.

### 3.1.2 GMF conditioning and updating based on instrumental recordings

Before producing GMFs following an earthquake using a suitably identified GMM and spatial correlation model, careful comparison of its predictions versus the actual observations recorded at the available stations in the region is necessary. This indicates how strong or weak the actual observations tended to be when compared to the mean GMM prediction. It is defined as the number of standard deviations by which an observed logarithmic intensity values differs from the mean logarithmic intensity values of a GMM at each site location where an actual recording is available.

For this study, these recorded instrumentations signals are provided by the Italian Accelerometric Archive (ITACA, http://itaca.mi.ingv.it) (Pacor et al. 2011a, b), where recordings belonging to a total of 64 and 118 stations for the Umbria-Marche and L'Aquila earthquakes, respectively, were considered. Figure 7 illustrates the observed ground motions from the 1st events of the 2009 L'Aquila and 1997 Umbria-Marche sequences registered within the ITACA database in comparison with the unadjusted Bindi et al. (2011) GMM for $Sa(T = 0.25$ s). The variability in the observations is consistent with the Bindi et al. (2011) model, as indicated by the $\pm 1\sigma$ and $\pm 2\sigma$ lines. However, some observations are slightly lower than the mean prediction. Therefore, to adjust for the number of standard deviations (+ or −) influencing the mean prediction yielded by the GMM based on the observations

which were registered at the stations, GMM conditioning is carried out. GMM conditioning essentially refines the inter-event variability term, since all observations come from the same earthquake rupture. Additionally, the impact of GMM conditioning can be further evaluated quantitatively by scrutinising the residuals with respect to the mean prediction as illustrated in Fig. 7c, d.

The conditioning of the ground shaking is based on the methodology developed by Douglas and Edwards (2016) and has been used in various regional seismic risk applications (Miano et al. 2016, 2020). To do this, the vector of the mean values $\boldsymbol{M}$ and the covariance matrix $\boldsymbol{\Sigma}$ previously presented is partitioned as follows:

$$\boldsymbol{M} = \begin{bmatrix} \boldsymbol{M}_1 \\ \boldsymbol{M}_2 \end{bmatrix} \tag{15}$$

$$\boldsymbol{\Sigma} = \begin{bmatrix} \boldsymbol{\Sigma}_{11} & \boldsymbol{\Sigma}_{12} \\ \boldsymbol{\Sigma}_{21} & \boldsymbol{\Sigma}_{22} \end{bmatrix} \tag{16}$$

where $\boldsymbol{M}_1$ is the mean vector of intensities for the sites of interest (e.g., building locations) calculated using the chosen GMM, and $\boldsymbol{M}_2$ is the mean vector of the calculated intensities for the stations where actual recordings are available within the area of interest calculated using the GMM. $\boldsymbol{\Sigma}_{11}$ is the covariance matrix for the calculated intensities for the sites of interest, $\boldsymbol{\Sigma}_{12} = \boldsymbol{\Sigma}_{21}$ is the cross-covariance matrix for the intensity values calculated at the sites and those calculated at the stations, $\boldsymbol{\Sigma}_{22}$ is the covariance matrix for the intensity values calculated at the actual recording stations. The conditional distribution of the logarithms of the calculated intensities values given the registered intensities values at the station is a joint normal distribution with a mean vector $\boldsymbol{M}_{1|2}$ and a covariance matrix $\boldsymbol{\Sigma}_{11|22}$:

$$\boldsymbol{M}_{1|2} = \boldsymbol{M}_1 + \boldsymbol{\Sigma}_{12}.\boldsymbol{\Sigma}_{22}^{-1}.(\mathbf{A}_2 - \boldsymbol{M}_2) \tag{17}$$

$$\boldsymbol{\Sigma}_{11|22} = \boldsymbol{\Sigma}_{11} - \boldsymbol{\Sigma}_{12}.\boldsymbol{\Sigma}_{22}^{-1}.\boldsymbol{\Sigma}_{21} \tag{18}$$

where $\mathbf{A}_2$ is the vector of the registered intensities values for the stations. In this study, the procedure outlined in Eqs. 12–18 is repeated for each spectral intensity within the range of $Sa_{avg}$ as defined previously in Eq. 2 and for all possible rupture scenarios reported in Table 5 to compute the required GMFs.

### 3.1.3 Calculation of average spectral acceleration-based GMFs

To calculate the values for the average spectral acceleration for each GMF, the indirect approach highlighted in Kohrangi et al. (2018) was used. This approach intends to bypass the current need to develop a GMM for $Sa_{avg}$ and its corresponding spatial correlation terms, and to make use instead of the existing models for $Sa(T)$ to 'indirectly' predict the $Sa_{avg}$ distribution. Given the joint lognormal distribution of spectral accelerations at different periods for any given scenario (Baker and Jayaram 2008), and the assumption of lognormality of $Sa_{avg}$ distribution, the mean and standard deviation can be indirectly estimated according to Eqs. 19 and 20 respectively:

$$\mu_{lnSa_{avg}} = \frac{1}{n}\sum_{l=1}^{n}\mu_{\mathrm{lnSa(T}_l)} \tag{19}$$

$$\sigma_{lnSa_{avg}} = \sqrt{\left(\frac{1}{n}\right)^2\sum_{l=1}^{n}\sum_{j=1}^{n}\rho_{\mathrm{lnSa(T}_l),\mathrm{lnSa(T}_m)}\sigma_{\mathrm{lnSa(T}_l)}\sigma_{\mathrm{lnSa(T}_m)}} \tag{20}$$

where $\mu_{\mathrm{lnSa(T}_l)}$ and $\sigma_{\mathrm{lnSa}(T_m)}$ are the logarithmic mean and total standard deviation obtained from a $Sa(T)$-based GMM such as Bindi et al. (2011).

Subsequently, the matrix $\boldsymbol{M}$ is now re-populated with logarithmic mean ground shaking intensity expressed in terms of $Sa_{avg}$ (from Eq. 19) whereas the covariance matrix $\boldsymbol{\Sigma}$ is re-calculated for $Sa_{avg}$ using the total standard deviation values associated with the logarithmic mean of $Sa_{avg}$ (from Eq. 20) and assuming that the inter- and intra-event variabilities are equal for all $Sa(T)$ values in Eq. 13.

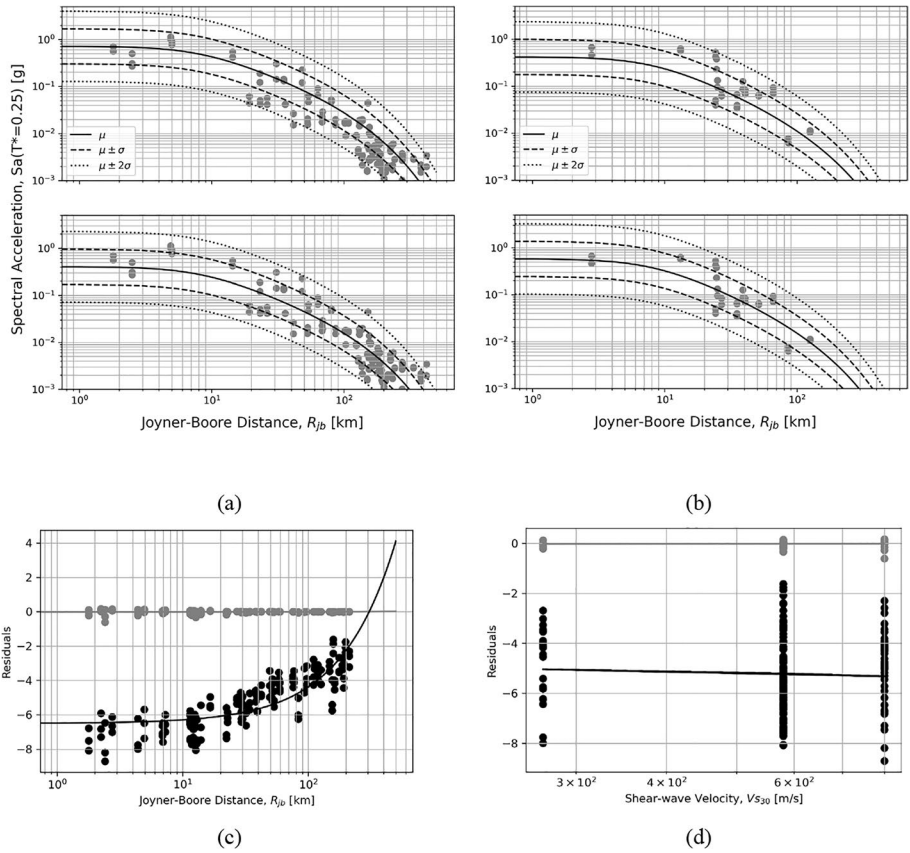


**Fig. 7** $Sa(T=0.25$ s) values of observed ground motions before (top) and after (bottom) the adjustment to the mean and standard deviation resulting from the between-event residuals of the **a** Umbria-Marche 1997 and **b** L'Aquila 2009 events; Comparison in residuals trends before (black scatter and line) and after (grey scatter and line) the application of GMM conditioning as a function of the **c** Joyner-Boore Distance for the L'Aquila 2009 event and **d** the average shear-wave velocities for the Umbria-Marche 1997 event

However, prior to the realisation of the $Sa_{avg}$-based GMFs, a verification exercise was carried out to demonstrate the robustness of the presented procedure in terms of reproducibility and accurate representation of GMFs with respect to those produced by national organisations. To this end, PGA-based GMFs were plotted against GMFs that were generated by the INGV for the L'Aquila 2009 event. GMFs were not simulated by the INGV prior to 2006 and therefore the Umbria-Marche event was not considered for this verification, though the predicted PGA-based GMF was plotted nevertheless. The INGV-based GMFs were produced using the Bindi et al. (2011) GMM considered in this study, ensuring a consistent comparative assessment. To give an example, the GMFs generated by the INGV reported a maximum PGA of 0.41 g whereas the GMFs produced here reported 0.42 g. Figure 8 illustrates the intensity footprints of the two GMFs, which are similar.

Given the previous comparison in Fig. 7 has shown the adequacy of the GMF production approach adopted here with respect to those produced by national authorities, it is extended to the intensity of interest for this study. In the future, such national authorities may consider also producing GMFs (i.e., ShakeMaps) for these next-generation IMs that have been repeatedly shown to be efficient predictors of seismic vulnerability in structures. The GMFs for the two earthquake sequences are presented in Fig. 9 where the average spectral acceleration fields are plotted alongside the epicentres. These intensity fields represent the mean ground shaking intensities of 10,000 GMF simulations.

### 3.2 Damage characterisation

Following the identification of the shaking intensities at each site location of interest in the region during several past earthquakes, the observed damage can be used in tandem with these to construct empirical FFs. Therefore, this section explores data collected for several buildings following the Umbria-Marche and L'Aquila earthquake sequences with the objective of developing such FFs.

In this study, the Database of Observed Damage (DaDO) (Dolce et al. 2019) was used, which is an online database maintained by the Eucentre Foundation and readily available on https://egeos.eucentre.it/danno_osservato/web/danno_osservato?lang=EN. It contains information on the structural characteristics and the observed damage of buildings inspected after the most relevant earthquakes in Italy from the Friuli 1976 event onwards. For the two events examined in the present study, the distribution of inspected building attributes is shown in Fig. 10, differentiating the buildings as a function of the period of construction, number of storeys and DSs recorded. It can be seen that the majority of the buildings were constructed around the 1970s and tended to be low-rise structures with five or fewer storeys. Regarding the DSs, it can be seen that the observed damage tended to be mild to moderate for the majority of cases, which will be discussed next.

The aforementioned data was available for over 122,574 buildings in two major earthquakes in recent history out of which, approximately 10,666 were RC buildings with masonry infills. These buildings were inspected visually by experts following the earthquakes with several general criteria. For nearly a century, seismologists have relied on macro-seismic intensity as the primary method to describe the impact or severity of ground shaking during earthquakes at specific locations in terms of observed damage (Mese et al. 2023). In 1998, the European macro-seismic scale (1998) (referred to as EMS-98) was commissioned and it is currently the standard basis for evaluation of seismic damage intensity evaluation in European countries and in a number of countries outside Europe. However, in Italy, the DSs illustrated in Fig. 10c, f and adopted in the DaDO database

correspond to the AeDES (*Agibilità e Danno nell'Emergenza Sismica*) standardised damage identification survey which was introduced in 1997. The AeDES survey form was initially introduced in 1997 when inspections were aimed to investigate primarily the vulnerability and damage to buildings (i.e., inspection of load-bearing elements). Subsequent changes were introduced in 2002 to look beyond safeguarding human life and hence focused on usability evaluation through the inclusion of damage to non-structural elements (i.e., infills). This update is evident in Fig. 10c, f where the Umbria-Marche event of 1997 accounts solely for the damage to the vertical structure whereas the L'Aquila 2009 event accounts for damage to both structural and non-structural system. The AeDES survey has been officially recognised by the Italian Department of Civil Protection (DPC) as the primary operational tool for managing technical aspects during emergencies (Baggio et al. 2002; Dolce et al. 2014).

Although the damage metric is based on the EMS-98 scale, the DSs associated with the AeDES form are grouped as follows for expedite surveys: D0 (no damage), D1 (slight), D2-D3 (moderate), D4-D5 (severe). For the Umbria-Marche and L'Aquila events, the DaDO database classified the surveyed buildings into their respective DS bins and this classification is described in Table 6.

Prior to analysing this damage data for the buildings in Umbria-Marche and L'Aquila, some form of a relationship between analytical and empirical DSs is required. This is due to the discrepancy between the criteria used to characterise the analytical FFs according to the Italian national code discussed in Sect. 2.5.3 versus the damage scales described in Table 6. To define such a correspondence between the limit states, some assumptions were needed based on the primary objectives of both. The correspondence is summarised in Table 7, with the justification in each case noted as follows:

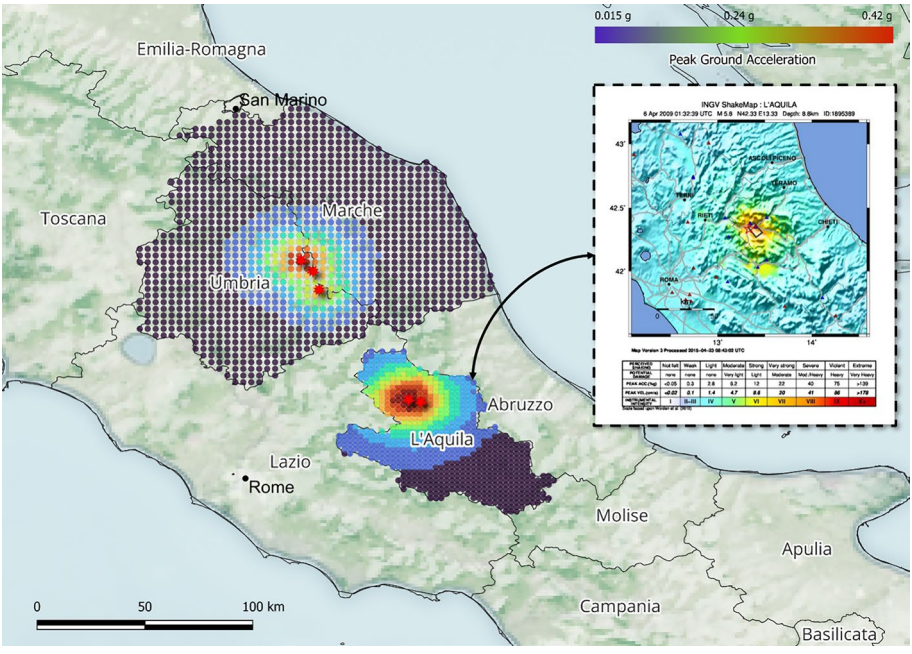


**Fig. 8** Comparison of PGA-based GMFs generated by the INGV and via the procedure adopted in this study for the L'Aquila 2009 event

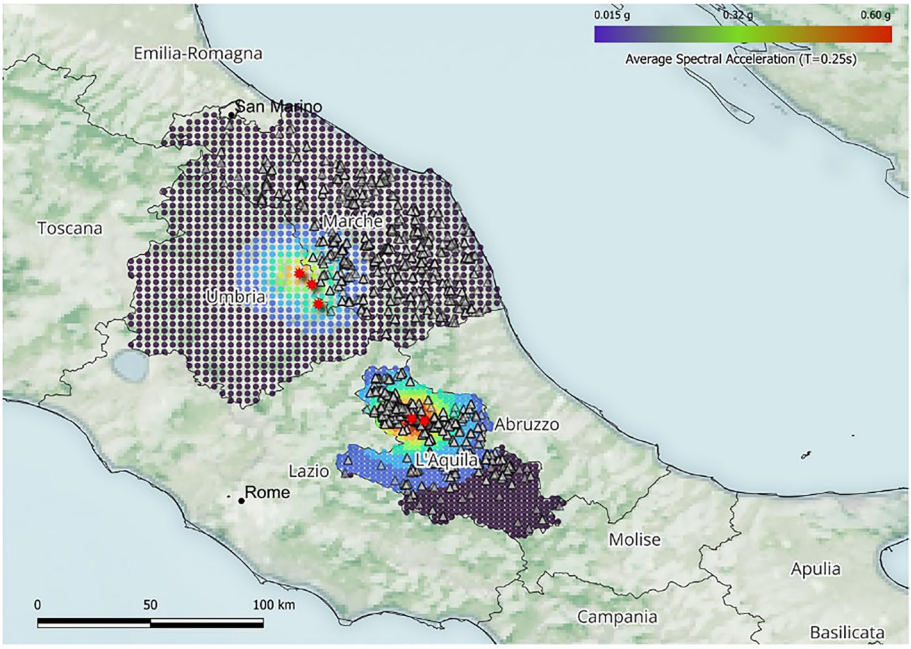


(a)

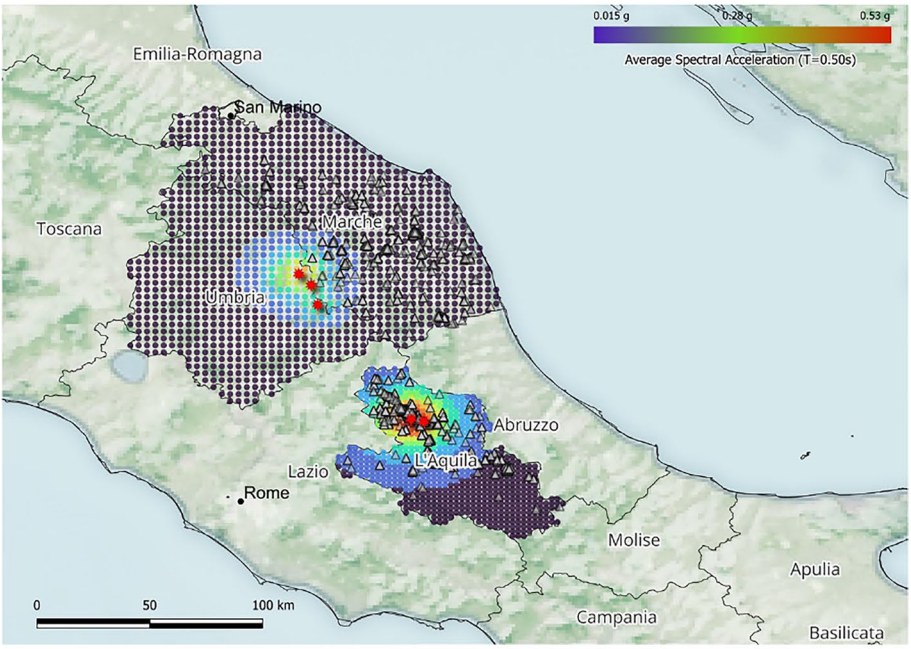


(b)

**Fig. 9** Ground-motion fields of the L'Aquila 2009 and Umbria-Marche 1997 events expressed in terms of the average spectral acceleration intensities conditioned on $T^* = 0.25$ s (**a**) and $T^* = 0.50$ s (**b**) (triangles represent the low and mid-rise buildings associated with the considered IMs)

- SLO corresponds to AeDES damage state D0 (Negligible Damage). Both focus on maintaining the functionality and usability of the building. Under SLO, the building should experience minor or negligible damage and remain functional, which is similar to D0, where the damage is considered negligible.
- SLD is akin to AeDES damage state D1 (Limited Damage). Both prioritise safety and immediate occupancy. In SLD, the building may sustain minor damage but remains safe for occupancy, which aligns with D1 where limited damage is allowed.
- SLV relates to AeDES damage state D2 (Moderate Damage). SLV aims to protect occupants' lives and ensures that they can egress safely, even with moderate damage. D2 reflects this by allowing for moderate damage while still maintaining life safety for occupants.
- SLC aligns with AeDES damage states D3 (Extensive Damage) and D4 (Severe Damage). In SLC, the primary objective is to prevent structural collapse, even if extensive or severe damage occurs. D3-D4 reflect this by allowing for substantial damage without immediate collapse.
- The additional collapse limit state aligns with the AeDES damage state D5 due to the fact that D5 accounts only for surveyed buildings which have fully collapsed.

### 3.3 Empirical fragility functions

To derive empirical FFs, the ground-shaking was characterised at every building site using the $Sa_{avg}$-based GMFs reported in Fig. 9. Since many of the buildings in the empirical database were subjected to several shaking events within the same earthquake (Table 5), the maximum value among all recorded events was used as the intensity value to pair with the damage observation. It is worth noting that using the maximum value among all recorded events (i.e., envelope of GMFs corresponding to all events within a sequence) as the intensity value for the damage observed in a particular building is an approximation. This approximation was assumed due to the difficulty in accurately quantifying with

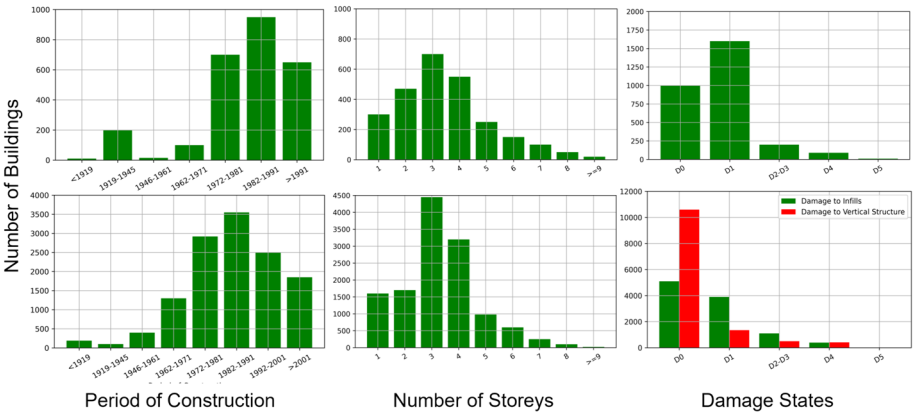


**Fig. 10** Distribution of attributes for the Umbria-Marche (top) and L'Aquila (bottom) surveyed damaged buildings

**Table 6** AeDES damage scales for structural and non-structural building elements based on EMS-98

| AeDES damage scales | EMS-98 damage scales | | Structural damage | Non-Structural damage |
|---|---|---|---|---|
| D0 | Grade 0 (DS0) | No damage | No | No |
| D1 | Grade 1 (DS1) | Negligible to slight damage | No | Slight |
| D2-D3 | Grade 2 (DS2) | Moderate damage | Slight | Moderate |
| | Grade 3 (DS3) | Substantial to heavy damage | Moderate | Heavy |
| D4-D5 | Grade 4 (DS4) | Very heavy damage | Heavy | Very heavy |
| | Grade 5 (DS5) | Destruction | Very heavy | Very heavy |

**Table 7** Proposed correspondence between the adopted analytical limit states and AeDES damage states and description of the primary objectives of both

| AeDES damage state | NTC2018 limit state | Primary objective |
|---|---|---|
| D0 | SLO | Functionality and usability of the building |
| D1 | SLD | Safety and immediate occupancy; |
| D2–D3 | SLV | Protection of occupants' lives and ensurance of safe evacuation |
| D4 | SLC | Structural collapse prevention; |
| D5 | Collapse | Structural collapse |

certainty the extent of damage caused by the multiple shaking events that occurred between the mainshock and the inspection time. The consequences of this approximation are further highlighted in detail in Sect. 4.

The derivation of FFs requires an appropriate statistical model and fitting technique to approximate observational data as a function of the ground motion severity. In line with existing literature studies (Rota et al. 2008; Gaudio et al. 2017; Ader et al. 2020) and similar to the analytical FF application in previous sections, the cumulative lognormal distribution is adopted for describing the probability of exceeding a preselected damage level, as a function of the seismic intensity measure, as per Eq. 10. Before to estimating the parameters of the lognormal fit and given the availability of building-by-building data, the Bernoulli sequence (Ioannou et al. 2015; Rossetto et al. 2014) is selected for characterising the random component of the statistical model (i.e., the probability of exceedance). This is primarily due to the individual buildings and damage observations all corresponding to a different intensity value; hence, is not possible to count the number of exceedances observed for several stripes of intensity, as in the case of MSA. The adoption of the Bernoulli sequence therefore avoids aggregating damage data into bins, which may introduce other issues (Ioannou et al. 2015; Rossetto et al. 2014). This Bernoulli sequence is defined via a binomial distribution as follows:

$$P(DS = ds_i|IM = im_j) = \binom{n_j}{y_{ij}} p_{ij}{}^{y_{ij}}[1 - p_{ij}]^{(n_j - y_{ij})} \tag{21}$$

where $P(DS = ds_i|IM = im_j)$ is the term expressing the probability of exceeding damage state $ds_i$ given the intensity measure threshold $imj$ as a binary outcome taking the value of

1 if the damage level is attained (i.e. DS = dsi)) or 0 otherwise (i.e. DS ≠ dsi), *nj* is the number of independent trials where each trial results in either "success" (with probability $p_{ij}$) or a "failure" (with probability 1-$p_{ij}$), *pij* is thus the exceedance probability defined by Eq. 10. Using this approach, the FFs are simultaneously fitted via the maximum likelihood estimation approach and a unique constant dispersion value, $\beta$, is assumed for all damage states to prevent intersecting fragility curves (Rosti et al. 2023; Lallemant et al. 2015; Nguyen and Lallemant 2022). For each building typology, optimal parameters of the fragility model result from maximising the logarithm of the likelihood function:

$$\eta_{DS_i}, \beta_{DS_i} = argmax\left[\log\left(\prod_{i=1}^{nDS}\prod_{j=1}^{N}\frac{n_j!}{y_{ij}!\left(n_j - y_{ij}\right)}p_{ij}^{\ y_{ij}}(1-p_{ij})^{(n_j-y_{ij})}\right)\right] \tag{22}$$

where *nDS* is the number of damage levels and *N* is the number of data points. It should be noted, however, that Iervolino (2023) has recently highlighted some conceptual issues with the problem definition outlined above and the format in which GMF and empirical damage data tend to be available, discussing potential improvements that would generally result in an increased dispersion in the resulting fragility based on preliminary investigations. These developments may be incorporated in future work.

The empirical FFs in terms of median intensities and dispersions for all the infilled RC sub-taxonomies were subsequently characterised and are presented in Fig. 11, with the distribution parameters listed in Table 8. Due to the limited number of observed collapses (D5), it was not possible to draw conclusions about the FFs related to the collapse limit state. This finding aligns with the observations made by Liel and Lynch (2012), for instance.

## 4 Discussion

This section provides a comparative assessment of the FFs derived from the analytical and empirical methods previously described and applied to two past earthquakes in Italy. Table 8 reports the error as the difference between the empirical and analytical intensities over the empirical intensity.

A good match between analytical and empirical FFs with regards to the serviceability DSs (i.e., operational and damage limitation) was observed, with reasonable errors varying between 0 and 16%. This indicates that the analytical models are capable of reproducing the damage distributions associated with this building class for these initial DSs. For the life-safety and near-collapse DSs, it can be seen that the analytical FFs tended to consistently overestimate the median intensities, with respect to the empirical observations. In other words, analytical FFs indicate that buildings possess a higher level of resistance than they truly possess. Unfortunately, no conclusions could be drawn concerning the FFs associated with the collapse limit state due to the low number of observed collapses, which is consistent with the observations of Liel and Lynch (2012), for example. Additionally, the dispersion values associated with the fitted empirical $Sa_{avg}$-based fragilities were compared to dispersions considering conventional IMs such as $Sa(T_1)$ and PGA in Fig. 12. The comparison highlights the notable benefit of considering $Sa_{avg}$ as the principal IM for regional applications considering the significant reduction in the overall uncertainty for the considered building taxonomies. $Sa_{avg}$ consistently yielded lower estimates of uncertainty across distinct typologies whereas the dispersions associated with other IMs such as PGA and

$Sa(T_1)$, for example, were approximately 2.31 and 1.61 times that of $Sa_{avg}$, respectively, in the case of Umbria-Marche and nearly 2.35 and 1.58 times in the case of L'Aquila.

These similarities and discrepancies between the analytical and empirical FFs may be due to many reasons, which are discussed herein. The first relates to the quality of data, particularly for the 1997 Umbria-Marche earthquake sequences, and the AeDES form. Before 2002, there was a lack of inclusion of many distinct aspects that could provide more pinpointed information, aiding the surveyor in providing more complete information. The AeDES form exhibited numerous limitations affecting the quality of gathered data: the inability to encompass all potential structural component types; differentiating between certain building typologies; variability in structural configurations within the same building; and seismic behaviour variability among typologies that appeared similar aesthetically, leading to their equal classification, for example. These limitations were acknowledged and addressed by practitioners and governmental agencies by incorporating various sub-components into the revised AeDES form through various optimisation campaigns. The main focus of these optimisations was to reduce the time needed for each inspection by avoiding requesting hard-to-obtain information during visual post-earthquake assessments.

The second issue relates to the damage accumulation in buildings following earthquake sequences. The Umbria-Marche 1997 and L'Aquila 2009 were seismic sequences that consisted of many events. As such, the collection of damage observations by field experts was generally carried out, for safety reasons, following the conclusion of the earthquake sequences and not directly after the first event. This means that the building damage data was collected accounting for damage accumulated following the entire sequence. The effect of damage accumulation is typically demonstrated with a decrease in the median intensities (Iacoletti et al. 2023; Iervolino et al. 2020; Aljawhari et al. 2021), compared to the case if they had been subjected to a single event. This contributes to the observation that the analytical FFs tended to have higher median values for the more severe limit states, since the numerical models were not subjected to the same level of input energy as the actual buildings were. Additionally, it is not anticipated that the initial DSs would be very susceptible to this damage accumulation since they typically relate to the more elastic region of response, which is reflected in their good matching with the data. This further highlights the importance of input energy, hysteretic energy dissipation and proper ground motion record selection to characterise all pertinent features like duration and mainshock-aftershock sequences.

The third issue relates to the harmonisation in the DS definition between Italian code and macro-seismic scales discussed in Sect. 3.2. Establishing such a correspondence is a significant assumption and is not an easy task. On one hand, the Italian code offers quantitative criteria that can be easily read from a numerical model's analysis results, whereas the macro-seismic scales offer more qualitative interpretations. This lack of direct correspondence could therefore lead to stronger discrepancies in the resulting FFs if not characterised adequately.

The last issue relates to the possibility of bias in data collection due to the differences in DS perception from one expert to another. A damage assessment tends to be subjective and depends on the judgement of the evaluator, which may be perceived differently by another evaluator moments later. The damage reports available provide no additional information on the number of expert judgements per surveyed building, or to what level they were trained and are qualified, which would have helped understand the potential for bias and uncertainty in the evaluation. For example, it may be that engineers involved in academic lab testing systematically differ in their interpretation of a certain damage mechanism with respect to other engineers more involved in practice and day-to-day construction projects.

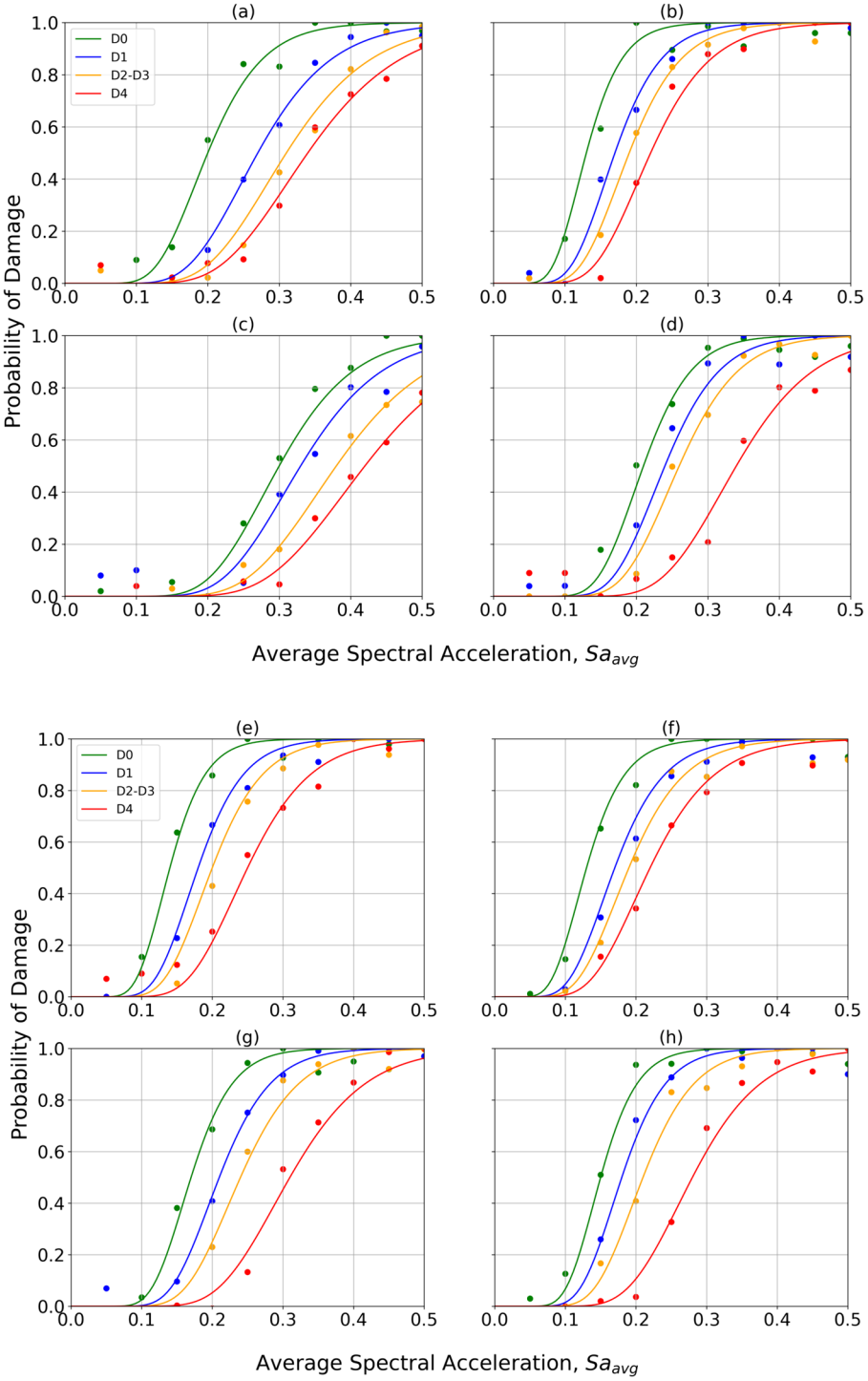


**Fig. 11** Typological empirical FFs derived for the L'Aquila (**a** LC-LR, **b** LC-MR, **c** MC-LR, **d** MC-MR) and the Umbria-Marche (**e** LC-LR, **f** LC-MR, **g** MC-LR, **h** MC-MR) events

**Table 8** Analytical and empirical fragility function parameters

| Sub-taxonomy | Analytical fragility functions | | | Empirical fragility functions | | | | | | | | |
|---|---|---|---|---|---|---|---|---|---|---|---|---|
| | | | | Damage state | L'Aquila 2009 | | | | Umbria-Marche 1997 | | | |
| | Damage state | $\tilde{\eta}_{DS_i}$ (g) | $\tilde{\beta}_{total\|DS_i}$ | | Building count | $\eta_{DS_i}$ (g) | $\beta_{DS_i}$ | Difference in median intensity [%]* | Building count | $\eta_{DS_i}$ (g) | $\beta_{DS_i}$ | Difference in median intensities [%]* |
| LC-LR | SLO | 0.20 | 0.43 | D0 | 399 | 0.20 | 0.30 | 0 | 113 | 0.14 | 0.28 | 43 |
| | SLD | 0.30 | | D1 | 437 | 0.27 | | 11 | 213 | 0.18 | | 67 |
| | SLV | 0.51 | | D2–D3 | 153 | 0.31 | | 65 | 32 | 0.20 | | 155 |
| | SLC | 0.67 | | D4 | 25 | 0.34 | | 97 | 7 | 0.25 | | 168 |
| | Collapse | 0.93 | | D5 | 0 | – | | – | 5 | – | | – |
| LC-MR | SLO | 0.13 | 0.48 | D0 | 689 | 0.13 | 0.30 | 0.00 | 125 | 0.13 | 0.32 | 0.00 |
| | SLD | 0.20 | | D1 | 278 | 0.17 | | 18 | 182 | 0.17 | | 18 |
| | SLV | 0.30 | | D2–D3 | 272 | 0.19 | | 58 | 15 | 0.19 | | 58 |
| | SLC | 0.50 | | D4 | 21 | 0.22 | | 127 | 1 | 0.22 | | 127 |
| | Collapse | 0.57 | | D5 | 1 | – | | – | 2 | – | | – |
| MC-LR | SLO | 0.22 | 0.46 | D0 | 1581 | 0.30 | 0.27 | − 27 | 345 | 0.17 | 0.27 | 29 |
| | SLD | 0.32 | | D1 | 1555 | 0.33 | | − 3 | 498 | 0.21 | | 52 |
| | SLV | 0.63 | | D2–D3 | 487 | 0.38 | | 66 | 54 | 0.24 | | 163 |
| | SLC | 0.72 | | D4 | 19 | 0.42 | | 71 | 4 | 0.31 | | 132 |
| | Collapse | 1.03 | | D5 | 3 | – | | – | 5 | – | | – |
| MC-MR | SLO | 0.14 | 0.48 | D0 | 689 | 0.21 | 0.25 | − 33 | 216 | 0.15 | 0.27 | − 7 |
| | SLD | 0.21 | | D1 | 1208 | 0.24 | | − 13 | 316 | 0.18 | | 17 |
| | SLV | 0.43 | | D2–D3 | 657 | 0.26 | | 65 | 26 | 0.21 | | 105 |
| | SLC | 0.49 | | D4 | 27 | 0.34 | | 44 | 2 | 0.28 | | 123 |
| | Collapse | 0.76 | | D5 | 1 | – | | – | 3 | – | | |

*Positive and negative values of the difference denote whether the analytical FFs overestimate or underestimate the seismic intensity, respectively

In any case, this subjectivity and bias tends to lead to an exaggeration in the observed damage, for a variety of reasons. One reason sometimes encountered is in order to qualify for government aid; hence, it is in the building owner's financial interest to exaggerate the damage suffered as much as possible in hopes of boosting their damage ranking and qualify for a higher financial pay-out to repair their building. The impact of this when translated to empirical FF development is that the median seismic intensities associated with the onset of each DS will tend to shift towards the left when compared to analytical FFs, which is what was observed in this study.

## 5 Conclusions

Fragility functions are used worldwide for single-building and regional seismic risk applications. They are typically the result of analytical campaigns comprising extensive nonlinear dynamic analyses or empirical damage data collected following past earthquakes.

In Italy, many notable studies have developed fragility functions (FFs) for various building taxonomies based on analytical and empirical data. However, these studies have tended to use traditional intensity measures (IMs), such as peak ground acceleration and spectral acceleration at a single period, and typically possess relatively high dispersion values. Reducing uncertainty via more efficient IMs is an essential step in improving seismic risk analyses. To address this issue, the novel IM average spectral acceleration, $Sa_{avg}$, was adopted and applied in this study. A comprehensive study to derive analytical FFs was carried out by first identifying the main attributes affecting the seismic vulnerability of reinforced concrete (RC) buildings and developing archetype numerical models. These were then classified into taxonomies to represent the Italian RC building stock by period of construction (i.e., low and moderate seismic code levels) and number of storeys (i.e., low- and mid-rise buildings). Damage states were defined reflecting the national building code and state-of-the-art experimental campaigns to adequately characterise the relationship between overall damage and the selected demand parameter values observed in the models, and subsequently derive FFs.

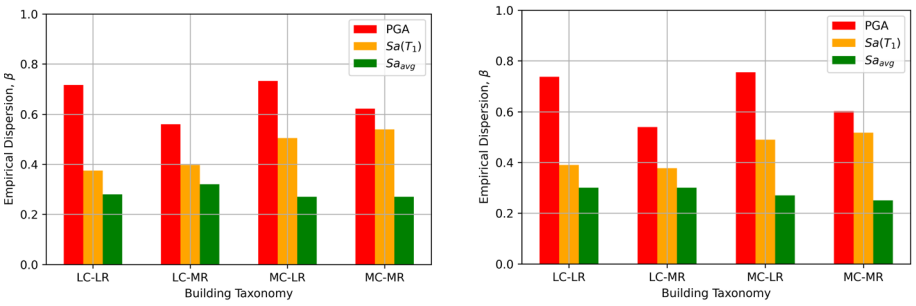


(a) L'Aquila 2009

(b) Umbria-Marche 1997

**Fig. 12** Dispersion values associated with the fitted empirical fragility functions considering the average spectral acceleration and other intensity measures such as peak ground acceleration and spectral acceleration

Empirical FFs were then derived using the database of observed damage (DaDO) compiled following field observations by the Eucentre Foundation. The steps required to derive FFs were highlighted with regards to the generation of ShakeMaps to quantify the ground-shaking intensity expressed in terms of $Sa_{avg}$ for the surveyed buildings pertaining to two events considered as case studies: Umbria-Marche 1997 and L'Aquila 2009. The estimated shaking at each building's site location in tandem with the observed damage state was used to develop the empirical FFs. These FFs expressed in terms of $Sa_{avg}$ represent a novel contribution to seismic risk applications for the Italian building stock using a more efficient IM.

Overall, when compared to empirical FFs, the analytical FFs tended to overestimate the median seismic intensities, more so for the more damaging limit states, yet assisted significantly in the reduction of overall dispersion when scrutinised with respect to other conventional IMs. The potential reasons for this difference were discussed and typically relate to issues of empirical damage data quality, the impacts of damage accumulation during successive sequences, the harmonisation of analytical damage state definitions and those used in post-earthquake inspections, and lastly related to possible instances of subjectivity and bias in data collection. All in all, this study provides an example on how such analytical and empirical data can be utilised in a more productive fashion via novel intensity measures and thorough analysis methods to provide reliable and robust FFs for future risk assessments and loss analyses.

## Appendix: Derivation of total uncertainty

The variance due to record-to-record (RTR) variability for a building "*j*" fragility is denoted as follows:

$$\beta^2_{RTR,j}$$

and the variance due to modelling (MDL) uncertainty is defined as follows:

$$\beta^2_{MDL}$$

The RTR and MDL variances are combined to get the adjusted (ADJ) fragility function, where the increase in variance is assumed to be constant for all buildings ($\beta_{MDL} = 0.34$). Assuming the record-to-record variability and modelling uncertainty are independent ($\rho = 0$), then the following can be written for the total uncertainty, as described in O'Reilly and Sullivan (2018), among others:

$$\beta^2_{ADJ,j} = \beta^2_{RTR,j} + \beta^2_{MDL} - 2\rho\beta_{RTR,j}\beta_{MDL} \tag{23}$$

$$\beta^2_{ADJ,j} = \beta^2_{RTR,j} + \beta^2_{MDL} \tag{24}$$

### Case A: Without modelling uncertainty

If the modelling uncertainty is ignored, the following equations hold to combine the inter- and intra-building uncertainties together to get the total fragility function

uncertainty and considering all buildings across $N$ buildings in a building class, as described in Ruggieri et al. (2021), among others:

$$\beta_{total}^2 = \beta_{intra}^2 + \beta_{inter}^2 \tag{25}$$

where

$$\beta_{intra}^2 = \frac{1}{N}\sum_{j=1}^{N}\beta_{RTR,j}^2 \tag{26}$$

$$\beta_{inter}^2 = \frac{1}{N}\sum_{j=1}^{N}\left(\ln\eta_j - \frac{1}{N}\sum_{j=1}^{N}\ln\eta_j\right)^2 \tag{27}$$

### Case B: With modelling uncertainties

If the modelling uncertainty is explicitly considered and assuming that it is a constant value that will only impact the dispersion while median values associated with the fragilities remain the same, this means only the intra term is impacted. As such, Eq. (26) can be rewritten as:

$$\beta_{intra,ADJ}^2 = \frac{1}{N}\sum_{j=1}^{N}\beta_{ADJ,j}^2 \tag{28}$$

where the variance has been inflated to accounted for modelling uncertainty.

If the adjusted intra-building variance (from Eq. 28) is then inserted into the term to compute the total variance (from Eq. 25), we now have:

$$\beta_{total,ADJ}^2 = \beta_{intra,ADJ}^2 + \beta_{inter}^2 \tag{29}$$

$$\beta_{total,ADJ}^2 = \frac{1}{N}\sum_{j=1}^{N}\beta_{ADJ,j}^2 + \beta_{inter}^2 \tag{30}$$

Expanding the adjusted term (from Eq. 30) to its individual components yields:

$$\beta_{total,ADJ}^2 = \frac{1}{N}\sum_{j=1}^{N}\left(\beta_{RTR,j}^2 + \beta_{MDL}^2\right) + \beta_{inter}^2 \tag{31}$$

and since the $\beta_{MDL}^2$ term is assumed constant for all buildings, it can be taken outside of the summation in Eq. (31) to give:

$$\beta_{total,ADJ}^2 = \frac{1}{N}\sum_{j=1}^{N}\beta_{RTR,j}^2 + \beta_{inter}^2 + \beta_{MDL}^2 \tag{32}$$

**Table 9** The numerical application presented herein applies the derivation presented earlier and expands on the results reported in Table 4 and associated with the collapse fragility of the LC-LR building class

| Building j | Median collapse intensity [g] | Mean collapse intensity [g] | Deviation from mean intensity prediction | Modelling variance, $\beta^2_{MDL}$ | Record-to-record variability, $\beta_{RTR,j}$ | Record-to-record variance, $\beta^2_{RTR,j}$ | Adjusted variance $\beta^2_{ADJ,j}$ | Adjusted intra-building variance $\beta^2_{intra,ADJ}$ | Inter-building variance $\beta^2_{inter}$ | Total variance, $\beta^2_{total,ADJ}$ | Total variability, $\beta_{total,ADJ}$ |
|---|---|---|---|---|---|---|---|---|---|---|---|
| 1 | 1.27 | 1.0078 | 0.069 | 0.12 | 0.37 | 0.14 | 0.25 | 0.11 | 0.037 | 0.26 | 0.51 |
| 2 | 0.79 | | 0.047 | | 0.38 | 0.14 | 0.14 | | | | |
| 3 | 1.07 | | 0.004 | | 0.27 | 0.073 | 0.073 | | | | |
| 4 | 0.74 | | 0.072 | | 0.33 | 0.109 | 0.109 | | | | |
| 5 | 1.16 | | 0.023 | | 0.34 | 0.12 | 0.12 | | | | |
| 6 | 0.84 | | 0.028 | | 0.32 | 0.10 | 0.10 | | | | |
| 7 | 1.21 | | 0.041 | | 0.25 | 0.063 | 0.063 | | | | |
| 8 | 0.85 | | 0.025 | | 0.27 | 0.073 | 0.073 | | | | |
| 9 | 1.22 | | 0.045 | | 0.29 | 0.084 | 0.084 | | | | |
| 10 | 0.9 | | 0.012 | | 0.27 | 0.073 | 0.073 | | | | |
| 11 | 1.19 | | 0.033 | | 0.37 | 0.14 | 0.14 | | | | |
| 12 | 0.85 | | 0.025 | | 0.32 | 0.10 | 0.10 | | | | |
| 13 | 1.22 | | 0.045 | | 0.32 | 0.10 | 0.10 | | | | |
| 14 | 0.8 | | 0.043 | | 0.28 | 0.078 | 0.078 | | | | |

$$\beta^2_{total,ADJ} = \beta^2_{intra} + \beta^2_{inter} + \beta^2_{MDL} \quad (33)$$

which is the same as the expression not considering modelling uncertainty, but with the $\beta^2_{MDL}$ simply added to the total variance to get the adjusted fragility function term.

In the case where the median values are impacted and the increased in dispersion is not fixed for all buildings, this simplification cannot be used and the intra and inter terms need to be individually adjusted before combination to get the total (Table 9).

**Author contributions** Both authors contributed to the study conception and design. Material preparation, data collection and analysis were performed by AMBN. The first draft of the manuscript was written by AMBN and GJO commented and edited on subsequent versions of the manuscript. Both authors read and approved the final manuscript.

**Funding** The work presented in this paper has been developed within the framework of the Projects "Dipartimenti di Eccellenza", funded by the Italian Ministry of Education, University and Research at IUSS Pavia.

**Data availability** The building models used as part of this study are freely available on Github at: https://github.com/gerardjoreilly/Infilled-RC-Building-Database, The data used to construct empirical fragility functions is available at the Database of Observed Damage (DaDO)at: https://egeos.eucentre.it/danno_osservato/web/danno_osservato?lang=EN.

**Code availability** No specific code was developed for general distribution as part of this study.

## Declarations

**Conflict of interest** The authors have no conflict of interest to declare that are relevant to the content of this article.

## References

Abarca A, Monteiro R, O'Reilly GJ (2022) Exposure knowledge impact on regional seismic risk assessment of bridge portfolios. Bull Earthq Eng 20(13):7137–7159. https://doi.org/10.1007/s10518-022-01491-z

Adachi T, Ellingwood BR (2009) Serviceability assessment of a municipal water system under spatially correlated seismic intensities. Comput Aided Civ Infrastruct Eng 24(4):237–248. https://doi.org/10.1111/j.1467-8667.2008.00583.x

Ader T, Grant DN, Free M, Villani M, Lopez J, Spence R (2020) An unbiased estimation of empirical lognormal fragility functions with uncertainties on the ground motion intensity measure. J Earthq Eng 24(7):1115–1133. https://doi.org/10.1080/13632469.2018.1469439

Aljawhari K, Gentile R, Freddi F, Galasso C (2021) Effects of ground-motion sequences on fragility and vulnerability of case-study reinforced concrete frames. Bull Earthq Eng 19(15):6329–6359. https://doi.org/10.1007/s10518-020-01006-8

ATC (2009) Quantification of building seismic performance factors

Baggio C, Bernardini A, Colozza R, Corazza L, Della Bella M, Di Pasquale G et al (2002) Manuale per la compilazione della Scheda di primo livello di rilevamento del danno, pronto intervento e agibilità per edifici ordinari nell'emergenza post-sismica (AeDES). Roma, Italy

Baker JW (2011) Conditional mean spectrum: tool for ground-motion selection. J Struct Eng 137(3):322–331. https://doi.org/10.1061/(ASCE)ST.1943-541X.0000215

Baker JW, Jayaram N (2008) Correlation of spectral acceleration values from NGA ground motion models. Earthq Spectra 24(1):299–317. https://doi.org/10.1193/1.2857544

Bindi D, Pacor F, Luzi L, Puglia R, Massa M, Ameri G et al (2011) Ground motion prediction equations derived from the Italian strong motion database. Bull Earthq Eng 9(6):1899–1920. https://doi.org/10.1007/s10518-011-9313-z

Borzi B, Pinho R, Crowley H (2008) Simplified pushover-based vulnerability analysis for large-scale assessment of RC buildings. Eng Struct 30(3):804–820. https://doi.org/10.1016/j.engstruct.2007.05.021

Bradley BA (2010) A generalized conditional intensity measure approach and holistic ground-motion selection. Earthq Eng Struct Dyn. https://doi.org/10.1002/eqe.995
Bradley BA, Dhakal RP (2008) Error estimation of closed-form solution for annual rate of structural collapse. Earthq Eng Struct Dyn 37(15):1721–1737. https://doi.org/10.1002/eqe.833
Cornell CA, Krawinkler H (2000) Progress and challenges in seismic performance assessment. PEER Center News 3(2):1–4
Crisafulli FJ, Carr AJ (2007) Proposed macro-model for the analysis of infilled frame structures. Bull N Z Soc Earthq Eng 40(2):69–77. https://doi.org/10.5459/bnzsee.40.2.69-77
Crowley H, Despotaki V, Silva V, Dabbeek J, Romão X, Pereira N et al (2021) Model of seismic design lateral force levels for the existing reinforced concrete European building stock. Bull Earthq Eng 19(7):2839–2865. https://doi.org/10.1007/s10518-021-01083-3
Danciu L, Nandan S, Reyes C, Basili R, Weatherill G, Beauval C et al (2021) EFEHR technical report 001: the 2020 update of the European Seismic Hazard Model: Model Overview. https://doi.org/10.12686/a15.
Dávalos H, Miranda E (2019) Filtered incremental velocity: a novel approach in intensity measures for seismic collapse estimation. Earthq Eng Struct Dyn 48(12):1384–1405. https://doi.org/10.1002/eqe.3205
De Biasio M, Grange S, Dufour F, Allain F, Petre-Lazar I (2014) A simple and efficient intensity measure to account for nonlinear structural behavior. Earthq Spectra 30(4):1403–1426. https://doi.org/10.1193/010614EQS006M
De Risi MT, Verderame GM (2017) Experimental assessment and numerical modelling of exterior non-conforming beam-column joints with plain bars. Eng Struct 150:115–134. https://doi.org/10.1016/j.engstruct.2017.07.039
De Risi MT, Ricci P, Verderame GM (2017) Modelling exterior unreinforced beam-column joints in seismic analysis of non-ductile RC frames. Earthq Eng Struct Dyn 46(6):899–923. https://doi.org/10.1002/eqe.2835
Del Gaudio C, Ricci P, Verderame GM, Manfredi G (2016) Observed and predicted earthquake damage scenarios: the case study of Pettino (L'Aquila) after the 6th April 2009 event. Bull Earthq Eng 14(10):2643–2678. https://doi.org/10.1007/s10518-016-9919-2
Del Gaudio C, De Martino G, Di Ludovico M, Manfredi G, Prota A, Ricci P et al (2017) Empirical fragility curves from damage data on RC buildings after the 2009 L'Aquila earthquake. Bull Earthq Eng 15(4):1425–1450. https://doi.org/10.1007/s10518-016-0026-1
Del Mese S, Graziani L, Meroni F, Pessina V, Tertulliani A (2023) Considerations on using MCS and EMS-98 macroseismic scales for the intensity assessment of contemporary Italian earthquakes. Bull Earthq Eng 21(9):4167–4189. https://doi.org/10.1007/s10518-023-01703-0
Dolce M, Papa F, Pizza AG (2014) Manuale per la compilazione della scheda di primo livello di rilevamento del danno, pronto intervento e agibilità per edifici ordinari nell'emergenza post-sismica (AeDES) seconda edizione. Roma, Italy
Dolce M, Speranza E, Giordano F, Borzi B, Bocchi F, Conte C et al (2019) Observed damage database of past Italian earthquakes: the Da.D.O. WebGIS. Bollettino Di Geofisica Teorica Ed Applicata. https://doi.org/10.4430/bgta0254
Dolšek M, Fajfar P (2008) The effect of masonry infills on the seismic response of a four-storey reinforced concrete frame—a deterministic assessment. Eng Struct 30(7):1991–2001. https://doi.org/10.1016/j.engstruct.2008.01.001
Douglas J, Edwards B (2016) Recent and future developments in earthquake ground motion estimation. Earth Sci Rev 160:203–219. https://doi.org/10.1016/j.earscirev.2016.07.005
Eads L, Miranda E, Krawinkler H, Lignos DG (2013) An efficient method for estimating the collapse risk of structures in seismic regions. Earthq Eng Struct Dyn 42(1):25–41. https://doi.org/10.1002/eqe.2191
Eads L, Miranda E, Lignos DG (2015) Average spectral acceleration as an intensity measure for collapse risk assessment. Earthq Eng Struct Dyn 44(12):2057–2073. https://doi.org/10.1002/eqe.2575
Esposito S, Iervolino I (2012) Spatial correlation of spectral acceleration in European data. Bull Seismol Soc Am 102(6):2781–2788. https://doi.org/10.1785/0120120068
European Standard (2004) Eurocode 8: design of structures for earthquake resistance—part 1: general rules, seismic actions and rules for buildings. European Committee for Standardization
Fardis MN, Calvi GM (1994) Effects of infills on the global response of reinforced concrete frames. In: Proceedings on the 10th European conference on earthquake engineering, Vienna, Balkema, Rotterdam
Grünthal G (ed) (1998) European Macroseismic Scale 1998 (EMS-98). Cahiers du Centre Européen de Géodynamique et de Séismologie, Luxembourg: Centre Européen de Géodynamique et de Séismologie. https://doi.org/10.2312/EMS-98.full.en
FEMA (2012) Seismic performance assessment of buildings. Volume 1. Methodology. Fema P-58-1

Fox MJ, O'Reilly GJ (2023) Exploring the site dependency of fragility functions in risk-targeted design. Earthq Eng Struct Dyn 52(13):4148–4163. https://doi.org/10.1002/eqe.3783
Gentile R, Calvi GM (2023) Direct loss-based seismic design of reinforced concrete frame and wall structures. Earthq Eng Struct Dyn 52(14):4395–4415. https://doi.org/10.1002/eqe.3955
Giordano N, De Luca F, Sextos A (2021) Analytical fragility curves for masonry school building portfolios in Nepal. Bull Earthq Eng 19(2):1121–1150. https://doi.org/10.1007/s10518-020-00989-8
Goda K, Atkinson GM (2009) Probabilistic characterization of spatially correlated response spectra for earthquakes in Japan. Bull Seismol Soc Am 99(5):3003–3020. https://doi.org/10.1785/012009007
Hak S, Morandi P, Magenes G, Sullivan TJ (2012) Damage control for clay masonry infills in the design of RC frame structures. J Earthq Eng 16(SUPPL. 1):1–35. https://doi.org/10.1080/13632469.2012.670575
Heresi P, Miranda E (2019) Uncertainty in intraevent spatial correlation of elastic pseudo-acceleration spectral ordinates. Bull Earthq Eng 17(3):1099–1115. https://doi.org/10.1007/s10518-018-0506-6
Heresi P, Miranda E (2021) Intensity measures for regional seismic risk assessment of low-rise wood-frame residential construction. J Struct Eng 147(1):04020287. https://doi.org/10.1061/(asce)st.1943-541x.0002859
Heresi P, Miranda E (2023) RPBEE: performance-based earthquake engineering on a regional scale. Earthq Spectra. https://doi.org/10.1177/87552930231179491
Iacoletti S, Cremen G, Galasso C (2023) Modeling damage accumulation during ground-motion sequences for portfolio seismic loss assessments. Soil Dyn Earthq Eng 168:107821. https://doi.org/10.1016/j.soildyn.2023.107821
Iervolino I (2023) Use and misuse of ShakeMap in (semi-) empirical fragility fitting. The 49th Risk, Hazard and Uncertainty Workshop, Hydra, Greece
Iervolino I, Chioccarelli E, Suzuki A (2020) Seismic damage accumulation in multiple mainshock–aftershock sequences. Earthq Eng Struct Dyn 49(10):1007–1027. https://doi.org/10.1002/eqe.3275
Ioannou I, Borg R, Novelli V, Melo J, Alexander D, Kongar I, Verucci E, Cahill B, Rossetto T (2012) The 29th May 2012 Emilia Romagna earthquakes, EPICentre Field Observation Report No. EPI-FO-290512
Ioannou I, Douglas J, Rossetto T (2015) Assessing the impact of ground-motion variability and uncertainty on empirical fragility curves. Soil Dyn Earthq Eng 69:83–92. https://doi.org/10.1016/j.soildyn.2014.10.024
Jalayer F, Cornell CA (2009) Alternative non-linear demand estimation methods for probability-based seismic assessments. Earthq Eng Struct Dyn 38(8):951–972. https://doi.org/10.1002/eqe.876
Jalayer F, De Risi R, Manfredi G (2015) Bayesian Cloud Analysis: efficient structural fragility assessment using linear regression. Bull Earthq Eng 13(4):1183–1203. https://doi.org/10.1007/s10518-014-9692-z
Jalayer F, Ebrahimian H, Miano A, Manfredi G, Sezen H (2017) Analytical fragility assessment using unscaled ground motion records. Earthq Eng Struct Dyn 46(15):2639–2663. https://doi.org/10.1002/eqe.2922
Jayaram N, Baker JW (2009) Correlation model for spatially distributed ground-motion intensities. Earthq Eng Struct Dyn 38(15):1687–1708. https://doi.org/10.1002/eqe.922
Karim Zadeh Z, Ghafory-Ashtiany M, Kalantari A, Shokuhirad S (2022) Development of analytical seismic fragility functions for the common buildings in Iran. Bull Earthq Eng 20(11):5905–5942. https://doi.org/10.1007/s10518-022-01411-1
Kohrangi M, Bazzurro P, Vamvatsikos D, Spillatura A (2017) Conditional spectrum-based ground motion record selection using average spectral acceleration. Earthq Eng Struct Dyn 46(10):1667–1685. https://doi.org/10.1002/eqe.2876
Kohrangi M, Kotha SR, Bazzurro P (2018) Ground-motion models for average spectral acceleration in a period range: Direct and indirect methods. Bull Earthq Eng 16(1):45–65. https://doi.org/10.1007/s10518-017-0216-5
Kohrangi M, Bazzurro P, Vamvatsikos D (2021) Seismic risk and loss estimation for the building stock in Isfahan: part II—hazard analysis and risk assessment. Bull Earthq Eng 19(4):1739–1763. https://doi.org/10.1007/s10518-020-01037-1
Krawinkler H, Miranda E (2004) Performance-based earthquake engineering. In: Bozorgnia Y, Bertero VV (eds) Earthquake engineering: from engineering seismology to performance-based engineering. CRC Press, Boca Raton
Kurukulasuriya M, Milanesi R, Bolognini D, Lanese I, Grottoli L, Magenes G et al (2022) Shaking table experimental campaign on pre-code masonry infills subjected to in-plane and out-of- plane loading. SPONSE, Stanford

Kurukulasuriya M, Milanesi R, Magenes G, Bolognini D, Grottoli L, Dacarro F et al (2023) Investigation of seismic behaviour of existing masonry infills through combined cyclic in-plane and dynamic out-of-plane tests. https://doi.org/10.7712/120123.10544.20695

Lallemant D, Kiremidjian A, Burton H (2015) Statistical procedures for developing earthquake damage fragility curves. Earthq Eng Struct Dyn 44(9):1373–1389. https://doi.org/10.1002/eqe.2522

Lee R, Kiremidjian AS (2007) Uncertainty and correlation for loss assessment of spatially distributed systems. Earthq Spectra 23(4):753–770. https://doi.org/10.1193/1.2791001

Liel AB, Lynch KP (2012) Vulnerability of reinforced-concrete-frame buildings and their occupants in the 2009 L'Aquila, Italy. Earthq Nat Hazards Rev 13(1):11–23. https://doi.org/10.1061/(ASCE)NH.1527-6996.0000047

Lin T, Haselton CB, Baker JW (2013) Conditional spectrum-based ground motion selection. Part I. Hazard consistency for risk-based assessments. Earthq Eng Struct Dyn 42(12):1847–1865. https://doi.org/10.1002/eqe.2301

Manfredi V, Masi A, Nicodemo G, Digrisolo A (2023) Seismic fragility curves for the Italian RC residential buildings based on non-linear dynamic analyses. Bull Earthq Eng 21(4):2173–2214. https://doi.org/10.1007/s10518-022-01605-7

Mangalathu S, Jeon JS (2020) Regional seismic risk assessment of infrastructure systems through machine learning: active learning approach. J Struct Eng 146(12):04020269. https://doi.org/10.1061/(asce)st.1943-541x.0002831

Marafi NA, Berman JW, Eberhard MO (2016) Ductility-dependent intensity measure that accounts for ground-motion spectral shape and duration. Earthq Eng Struct Dyn 45(4):653–672. https://doi.org/10.1002/eqe.2678

Markhvida M, Ceferino L, Baker JW (2018) Modeling spatially correlated spectral accelerations at multiple periods using principal component analysis and geostatistics. Earthq Eng Struct Dyn 47(5):1107–1123. https://doi.org/10.1002/eqe.3007

McKenna F (2011) OpenSees: a framework for earthquake engineering simulation. Comput Sci Eng 13(4):58–66. https://doi.org/10.1109/MCSE.2011.66

Miano A, Jalayer F, De Risi R, Prota A, Manfredi G (2016) Model updating and seismic loss assessment for a portfolio of bridges. Bull Earthq Eng 14(3):699–719. https://doi.org/10.1007/s10518-015-9850-y

Miano A, Jalayer F, Forte G, Santo A (2020) Empirical fragility assessment using conditional GMPE-based ground shaking fields: application to damage data for 2016 Amatrice Earthquake. Bull Earthq Eng 18(15):6629–6659. https://doi.org/10.1007/s10518-020-00945-6

Milanesi RR, Morandi P, Hak S, Magenes G (2021) Experiment-based out-of-plane resistance of strong masonry infills for codified applications. Eng Struct 242:112525. https://doi.org/10.1016/j.engstruct.2021.112525

MINISTERO DELLE INFRASTRUTTURE E DEI TRASPORTI (2019) CIRCOLARE 21 gennaio 2019 , n. 7 C.S.LL.PP. . Istruzioni per l'applicazione dell'Aggiornamento delle Norme tecniche per le costruzioni di cui al decreto ministeriale 17 gennaio 2018. Roma, Italy

Morandi P, Hak S, Magenes G (2018) Performance-based interpretation of in-plane cyclic tests on RC frames with strong masonry infills. Eng Struct 156:503–521. https://doi.org/10.1016/j.engstruct.2017.11.058

Morandi P, Hak S, Milanesi RR, Magenes G (2022) In-plane/out-of-plane interaction of strong masonry infills: from cyclic tests to out-of-plane verifications. Earthq Eng Struct Dyn 51(3):648–672. https://doi.org/10.1002/eqe.3584

Mori F, Mendicelli A, Moscatelli M, Romagnoli G, Peronace E, Naso G (2020) A new Vs30 map for Italy based on the seismic microzonation dataset. Eng Geol 275:105745. https://doi.org/10.1016/j.enggeo.2020.105745

Mucedero G, Perrone D, Monteiro R (2022) Epistemic uncertainty in poorly detailed existing frames accounting for masonry infill variability and RC shear failure. Earthq Eng Struct Dyn 51(15):3755–3778. https://doi.org/10.1002/eqe.3748

Nafeh AMB, O'Reilly GJ (2022) Unbiased simplified seismic fragility estimation of non-ductile infilled RC structures. Soil Dyn Earthq Eng 157:107253. https://doi.org/10.1016/j.soildyn.2022.107253

Nafeh AMB, O'Reilly GJ (2023) Simplified pushover-based seismic risk assessment methodology for existing infilled frame structures. Bull Earthq Eng. https://doi.org/10.1007/s10518-022-01600-y

Nguyen M, Lallemant D (2022) Order matters: the benefits of ordinal fragility curves for damage and loss estimation. Risk Anal 42(5):1136–1148. https://doi.org/10.1111/risa.13815

NTC (2018) Norme Tecniche Per Le Costruzioni. Rome, Italy

NTC IM of I and (2018) Norme Tecniche per le Costruzioni. DM 17/1/2018. Gazzetta Ufficiale Della Repubblica Italiana

O'Reilly GJ (2021) Limitations of Sa(T 1) as an intensity measure when assessing non-ductile infilled RC frame structures. Bull Earthq Eng 19(6):2389–2417. https://doi.org/10.1007/s10518-021-01071-7
O'Reilly GJ, Nafeh AMB (2021) Infilled-RC-building-database. GitHub Repos. https://doi.org/10.5281/zenodo.5082990
O'Reilly GJ, Sullivan TJ (2018) Quantification of modelling uncertainty in existing Italian RC frames. Earthq Eng Struct Dyn 47(4):1054–1074. https://doi.org/10.1002/eqe.3005
O'Reilly GJ, Sullivan TJ (2019) Modeling techniques for the seismic assessment of the existing Italian RC frame structures. J Earthq Eng 23(8):1262–1296. https://doi.org/10.1080/13632469.2017.1360224
O'Reilly GJ, Sullivan TJ, Monteiro R (2018) On the seismic assessment and retrofit of infilled RC frames structures. In: 16th European conference on earthquake engineering, Thessaloniki, Greece
O'Reilly GJ, Yasumoto H, Suzuki Y, Calvi GM, Nakashima M (2022) Risk-based seismic design of base-isolated structures with single surface friction sliders. Earthq Eng Struct Dyn 51(10):2378–2398. https://doi.org/10.1002/eqe.3668
Olteanu P, Coliba V, Vacareanu R, Pavel F, Ciuiu D (2016) Analytical seismic fragility functions for dual RC structures in Bucharest. https://doi.org/10.1007/978-3-319-29844-3_33
Pacor F, Paolucci R, Luzi L, Sabetta F, Spinelli A, Gorini A et al (2011a) Overview of the Italian strong motion database ITACA 10. Bull Earthq Eng 9(6):1723–1739. https://doi.org/10.1007/s10518-011-9327-6
Pacor F, Paolucci R, Ameri G, Massa M, Puglia R (2011b) Italian strong motion records in ITACA: overview and record processing. Bull Earthq Eng 9(6):1741–1759. https://doi.org/10.1007/s10518-011-9295-x
Padgett JE, DesRoches R, Nilsson E (2010) Regional seismic risk assessment of bridge network in Charleston, South Carolina. J Earthq Eng 14(6):918–933. https://doi.org/10.1080/13632460903447766
Pagani M, Monelli D, Weatherill G, Danciu L, Crowley H, Silva V et al (2014) Openquake engine: an open hazard (and risk) software for the global earthquake model. Seismol Res Lett 85(3):692–702. https://doi.org/10.1785/0220130087
Pagano M (1977) Teoria degli edifici: Edifici in cemento armato. vol. II. L
Parisi F, Luca F De, Petruzzelli F, De Risi R, Chioccarelli E (2012) Field inspection after the May 20th and 29th 2012 Emilia-Romagna earthquakes, available at http://www.reluis.it
Pavel F, Vacareanu R (2017) Spatial correlation of ground motions from vrancea (Romania) intermediate-depth earthquakes. Bull Seismol Soc Am 107(1):489–494. https://doi.org/10.1785/0120160095
Porter K, Kennedy R, Bachman R (2007) Creating fragility functions for performance-based earthquake engineering. Earthq Spectra 23(2):471–489. https://doi.org/10.1193/1.2720892
Qian J, Dong Y (2020) Multi-criteria decision making for seismic intensity measure selection considering uncertainty. Earthq Eng Struct Dyn 49(11):1095–1114. https://doi.org/10.1002/eqe.3280
Regio Decreto (1939) Norme per l'esecuzione di opere in conglomerato cementizio semplice o armato. Royal Decree
Rossetto T, Ioannou I, Grant DN, Maqsood N (2014) Guidelines for the empirical vulnerability assessment. GEM technical report, Pavia
Rosti A, Del Gaudio C, Rota M, Ricci P, Di Ludovico M, Penna A et al (2021) Empirical fragility curves for Italian residential RC buildings. Bull Earthq Eng 19(8):3165–3183. https://doi.org/10.1007/s10518-020-00971-4
Rosti A, Smerzini C, Paolucci R, Penna A, Rota M (2023) Validation of physics-based ground shaking scenarios for empirical fragility studies: the case of the 2009 L'Aquila earthquake. Bull Earthq Eng 21(1):95–123. https://doi.org/10.1007/s10518-022-01554-1
Rota M, Penna A, Strobbia CL (2008) Processing Italian damage data to derive typological fragility curves. Soil Dyn Earthq Eng 28(10–11):933–947. https://doi.org/10.1016/j.soildyn.2007.10.010
Rota M, Penna A, Strobbia C, Magenes G (2011) Typological seismic risk maps for Italy. Earthq Spectra 27(3):907–926. https://doi.org/10.1193/1.3609850
Ruggieri S, Porco F, Uva G, Vamvatsikos D (2021) Two frugal options to assess class fragility and seismic safety for low-rise reinforced concrete school buildings in Southern Italy. Bull Earthq Eng 19(3):1415–1439. https://doi.org/10.1007/s10518-020-01033-5
Ruggieri S, Calò M, Cardellicchio A, Uva G (2022) Analytical-mechanical based framework for seismic overall fragility analysis of existing RC buildings in town compartments. Bull Earthq Eng 20(15):8179–8216. https://doi.org/10.1007/s10518-022-01516-7
Ruggieri S, Liguori FS, Leggieri V, Bilotta A, Madeo A, Casolo S et al (2023) An archetype-based automated procedure to derive global-local seismic fragility of masonry building aggregates: METAFORMA-XL. Int J Disaster Risk Reduct 95:103903. https://doi.org/10.1016/j.ijdrr.2023.103903
Santarella L (1957) Il cemento armato: Le applicazioni alle costruzioni civili e industriali (in Italian). vol. II. H

SERA (2018) D26.2 Methods for developing European residential exposure
Shiraki N, Shinozuka M, Moore JE, Chang SE, Kameda H, Tanaka S (2007) System risk curves: probabilistic performance scenarios for highway networks subject to earthquake damage. J Infrastruct Syst 13(1):43–54. https://doi.org/10.1061/(ASCE)1076-0342(2007)13:1(43)
Silva V, Crowley H, Varum H, Pinho R (2015) Seismic risk assessment for mainland Portugal. Bull Earthq Eng 13(2):429–457. https://doi.org/10.1007/s10518-014-9630-0
Sokolov V, Wenzel F (2011) Influence of spatial correlation of strong ground motion on uncertainty in earthquake loss estimation. Earthq Eng Struct Dyn 40(9):993–1009. https://doi.org/10.1002/eqe.1074
Sousa R, Batalha N, Silva V, Rodrigues H (2021) Seismic fragility functions for Portuguese RC precast buildings. Bull Earthq Eng 19(15):6573–6590. https://doi.org/10.1007/s10518-020-01007-7
Vamvatsikos D, Cornell CA (2005) Developing efficient scalar and vector intensity measures for IDA capacity estimation by incorporating elastic spectral shape information. Earthq Eng Struct Dyn 34(13):1573–1600. https://doi.org/10.1002/eqe.496
Verdi VI a G, Cb AC, Famiglia FDI, Popolazione D, Abitazioni ED (2011) Censimento generale della popolazione e delle abitazioni, pp 1–24
Wang M, Takada T (2005) Macrospatial correlation model of seismic ground motions. Earthq Spectra 21(4):1137–1156. https://doi.org/10.1193/1.2083887
Wesson RL (2001) Spatial correlation of probabilistic earthquake ground motion and loss. Bull Seismol Soc Am 91(6):1498–1515. https://doi.org/10.1785/0120000284
Worden CB, Thompson EM, Hearne M, Wald DJ (2020) ShakeMap manual: technical manual, user's guide, and software guide. https://doi.org/10.5066/F7D21VPQ